THE ASTROPHYSICAL JOURNAL, 432:518–546, 1994 September 10

INFRARED IMAGING OF SPIRAL GALAXIES: COLORS AND LUMINOSITY PROFILES

DONALD M. TERNDRUP,[1,2,3] ROGER L. DAVIES,[4] JAY A. FROGEL,[1,3,5] D. L. DEPOY,[1,3,6] AND LISA A. WELLS[7]

Received 1993 December 29; accepted 1994 March 17

ABSTRACT

We present surface photometry of 43 S0 and spiral galaxies in the K band with a subset also observed in J. Most of the data are photometrically calibrated. We combine our data with published optical major-axis profiles to construct a set of galaxies with rJK colors, divide the major-axis profiles into bulge-dominated and disk-dominated regions, and compute mean colors and color gradients separately for bulges and disks. Typically the disk colors are measured from 0.8 to 1.8 scale lengths.

The colors of the bulge and disk components are strongly correlated, indicating that both components have a red stellar content that is similar in both age and metallicity. In the mean the disks are 0.1 mag bluer in $r-K$ than bulges; this color difference would arise if the disks are 2–4 $\times$ 10^9 yr younger or have lower metallicities by Δ[Fe/H] ≈ -0.1 to -0.2. Many of the bulges exhibit negative color gradients (bluer outward), which indicate that metallicity gradients of order Δ[Fe/H] ~ -0.2 may be common in bulges. Bulges of late-type galaxies are bluer on average than those of early types, probably a consequence of lower metallicity. About 25% of the galaxies have especially red bulge and disk colors, which we interpret as arising from large internal extinction rather than from an enhanced star-formation rate.

Subject headings: galaxies: photometry — galaxies: spiral — galaxies: stellar content — galaxies: structure — infrared: galaxies

1. INTRODUCTION

A multiwavelength survey of spiral galaxies which combines optical and infrared images can reveal much about the galaxies' morphology and stellar content. Near-IR images detect light primarily from cool giants and dwarfs which contribute the major fraction of the bolometric luminosity of a galaxy. Most spirals and S0 galaxies have an underlying population of such stars in their disks (e.g., Gregg 1989; Bothun & Gregg 1990). Particularly in spiral galaxies, cool giants are much better tracers of the mass distribution of a galaxy than are the bluer, hotter stars which delineate the spiral arms (Aaronson 1977; Frogel 1988).

Absorption and scattering by dust can also have a strong effect on the appearance and morphological classification of a galaxy; because the extinction of K (2.2 μm) is only one-tenth that at visible wavelengths, surveys in the infrared provide a better view of overall structure. Near-IR images can reveal significant structural features, such as bars, which are not visible on optical images. Examples are NGC 1068 (Scoville et al. 1988) and NGC 1566 (Hackwell & Schweizer 1983). As has been shown in the case of M51 (Rix 1993; Rix & Rieke 1993), optical and near-IR images together can map surface density enhancements in bars or spiral arms and distinguish these from variations in the number of hot stars.

Aaronson (1979) reported the first extensive photometric survey of spiral galaxies in the K-band and discovered that, when observed through large apertures dominated by disk light, most spirals have $V-K$ colors comparable to those of elliptical and lenticular galaxies but have substantially bluer $U-V$ colors. He also showed that spiral galaxies tend to have bluer $V-K$ colors with increasing aperture size. Aaronson's results were confirmed and extended by Griersmith, Hyland, & Jones (1982) who reported optical and infrared photometry of 65 early-type spiral galaxies through smaller apertures than those used by Aaronson. They noted that the colors of the inner region of these galaxies (which they associated with the bulge) are constant from de Vaucouleurs morphological type $T = -1$ (late S0) to $T = 3$ (Sb), but are bluer in later-type galaxies. They attributed the bluer optical colors of the late-type spirals to star formation in the spiral arms rather than to a trend to lower metallicity in later types.

We have begun a $BVRJHK$ survey with large-format optical and infrared arrays of $\sim$300 spiral and S0 galaxies chosen from A Revised Shapley-Ames Catalog of Bright Galaxies (Sandage & Tammann 1981, hereafter the RSA). The goals of our survey are to study the radial and azimuthal variations in extinction and stellar content, and to assemble a large sample of galaxies for the interpretation of galaxy colors at large redshift.

In this paper we report the initial results of a pilot study undertaken with the first generation of infrared arrays. For this study we have imaged the central regions of 43 spiral and S0 galaxies with a small format near-IR detector. In § 2 below, we describe our observational methods and data reduction techniques, establish the precision of our photometry, and discuss the determination of luminosity, color, ellipticity, and position angle profiles. Using our data in combination with r-band surface photometry from Kent (1984, 1986, 1987), we can separately characterize the colors of the bulges and disks (§ 3).

[1] Department of Astronomy, The Ohio State University, 174 West 18th Avenue, Columbus, OH 43120.
[2] Presidential Young Investigator; E-mail: terndrup@payne.mps.ohio-state.edu.
[3] Visiting Astronomer, Kitt Peak National Observatory, National Optical Astronomy Observatories, which is operated by the Assocation of Universities for Research in Astronomy, Inc. (AURA), under cooperative agreement with the National Science Foundation.
[4] Department of Physics, Astrophysics Group, Oxford University, Keble Road, Oxford OX1 3RH, UK; E-mail: rld@astro.ox.ac.uk.
[5] Visiting Research Associate, The Observatories of the Carnegie Institution of Washington; E-mail: frogel@payne.mps.ohio-state.edu.
[6] E-mail: depoy@payne.mps.ohio-state.edu.
[7] Cerro Tololo Inter-American Observatory, Casilla 603, La Serena, Chile. Postal address: KPNO/NOAO, P.O. Box 26732, Tucson, AZ 85726; E-mail: lwells@noao.edu.

Results of our analysis are discussed in § 4 and summarized in § 5.

2. OBSERVATIONS, DATA REDUCTION, AND ANALYSIS

2.1. *Selection and Observations of Galaxies*

The small format of infrared array detectors available to us in 1989 and 1990 led us preferentially to observe galaxies with small angular sizes ($D_{25} \leq 5'$), and to concentrate our investigation on the properties of their central regions. We generally selected galaxies that did not have an unusual morphology or were strongly barred, as judged from their appearance in the RSA. An additional criterion for selection was the availability of high quality optical surface photometry to compare with our near-IR observations. Most of our galaxies were therefore selected from Kent's (1984, 1986, 1987) papers. Finally, we added a few galaxies with box-peanut bulges and a few well-known edge-on systems.

The objects we observed are listed in the first column of Table 1. Column (2) gives the Hubble type T from de Vaucouleurs et al. (1991, hereafter the RC3); column (3) lists the morphological classification from the RSA when available or from de Vaucouleurs et al. (1991). About 70% of the sample are Sb or Sc galaxies, the remainder of earlier type.

The galaxies were observed during three observing runs in 1989 and 1990 on the 2.1 and 1.3 m telescopes at Kitt Peak. The instrument on both telescopes was the IRIM camera with a 58 × 62 pixel InSb detector (Fowler et al. 1987). On the 2.1 m telescope the camera was configured in 1:1 demagnification, producing a pixel scale of 0".54 pixel^{-1} and a field of view of 32". On the 1.3 m, the corresponding figures are 0.67:1 demagnification, 1".35 pixel^{-1}, and 81" field size.

Sky frames, taken well away from the location of the galaxy, were generally obtained before and after each galaxy observation. During each sequence of sky observations, the telescope position was dithered so that any stellar images would land on different places in the chip. At each of the sky or galaxy positions, we obtained from 4 to 20 exposures, with integration times set so that the mean sky level in K was 5000 to 10,000 counts (significant nonlinearities and saturation of the InSb detector occurred higher than 25,000 counts). This count level was achieved in 75–90 s on the 1.3 m and in 180 to 300 s on the 2.1 m. For equal exposure times the J frames went significantly deeper than the K frames because the sky brightness typically is 3 to 4 times lower than at K. Some observations were also obtained at H, but will not be discussed in this paper.

About half the nights devoted to this project on the 1.3 m were photometric. On these nights we obtained images at both J and K. On the nonphotometric nights we normally obtained images in K only, though for two galaxies we imaged in both J and K. Columns (4) and (5) of Table 1 list the total on-source exposure times for the 1.3 m observations in J and K, respectively, while column (8) designates the manner in which the galaxy images could be photometrically calibrated (see § 2.3). Galaxies with Kent's r-band photometry are indicated in column (9).

The purpose of the 2.1 m run was to observe the central regions of the galaxies at higher spatial resolution than on the 1.3 m. On the 2.1 m, the seeing was typically 1"–1".2 while on the 1.3 m the stellar seeing disks were almost always undersampled. The nights of the 2.1 m run were quite transparent but not photometric. On these nights, we obtained long exposure frames at J and K of several galaxies in order to achieve a high signal-to-noise ratio ($\geq$20 pixel^{-1}). The total on-galaxy exposure times for the 2.1 m observations are listed in columns (6) and (7) of Table 1.

For many of the large galaxies we observed a grid of images on the 1.3 m to increase the area over which we could perform surface photometry. Typically, we obtained on-source frames with a galaxy's nucleus centered on the frame, then we obtained others with the nucleus placed near the corners of the frame. The exposure times for all frames that made up the grid

TABLE 1

LOG OF OBSERVATIONS

			Exposure time (sec) 1.3 m		2.1 m				
NGC	T	classification	J	K	J	K	Phot	Opt	Notes
128	–2	S0$_2$(8)pec	480	720			s		
474	–2	RS0/a	450	1050			s	1	repeat
670	–2	Sb(s)I-II	240	840	1000	600	s	1	grid, repeat
697	5	[Sc]		760			s	1	grid
753	4	Sc(s)I-II		960	1200	700	s	2	
801	5	[Sc]	360	450			s	2	
891	3	Sb	450	450			s		grid
1023	–3	SB0$_1$(5)	180	90			s		
1035	5	Sc(s)III	450	450			s	2	
1087	5	Sc(s)III.3		1080			s	1,2	
1175	–1	S0$_2$(8)		540	2300	1200	s		grid
1325	4	SB(s)II		720			s	2	
1417	3	Sb(s)I.3	600	600	2300	1000	n	2	
1620	4	[Sbc]		720			s	2	
2654	2	Sab:		1800			s		
2681	0	Sa	400	600			n		
2715	5	Sc(s)II		480			n	2	
2742	5	Sc(rs)II		600			n	2	
2841	3	Sb	240	240			a	3	grid
2903	4	Sc(s)I-II		240			n	3	
3198	5	Sc(s)I-II		240			n	3	
3495	5	Sc(s)II-III		240			n	2	
3672	5	Sc(s)I-II		240			n		
4062	5	Sc(s)II-III		480			n	2	
4448	2	Sa(late)		240			n	2	
4565	3	Sb	240	240			a		grid
4800	3	Sb(rs)II-III		240			n	2	
5033	5	Sb(s)I	240	240			a	3	grid
5879	4	Sb(s)II		240			n		
7217	2	Sb(r)II-III	300	300			s	2	grid
7331	3	Sb(rs)I-II	450	540	1080	900	s	3	grid
7332	–2	S0$_{2/3}$(8)	240	720	1530	540	s		grid
7448	4	Sc(r)II.2	720	720	1200	600	s	1	
7457	–3	S0$_1$(5)	480	720			s		
7469	1	Sab		720			s	1	repeat
7537	4	[Sbc]	450	600	700	900	s	2	
7541	4	Sc(s)II	450	600			s	1,2	
7606	3	Sb(r)I		720			s	2	
7631	3	[Sb]		960			s	1	
7640	5	SBc(s)II:		960			s		
7664	5	[Sc]	600	720	1500	600	s	1,2	
7673	5	[Sc]	480	720	1300	1300	s	1	
7798	5	[Sc]		960	1200	600	s	1	
7814	2	S(ab)		720			s		
7817	4	[Sbc]		720			s	1	

NOTES.—Hubble type T is from de Vaucouleurs et al. 1991. Galaxy classification is from the RSA or from de Vaucouleurs et al. 1991; the latter designations are in square brackets. The notation "s" in col. (8) designates that the photometric calibration was via standards in Elias et al. (1982); "a" means that the galaxies were calibrated via aperture photometry in the literature and assumed airmass coefficients; "n" shows that the galaxies were observed under nonphotometric conditions. The references to optical photometry in col. (9) are (1) Kent 1984, (2) Kent 1986, (3) Kent 1987. In col. (10), "grid" means that a grid of observations were taken to increase the area sampled; "repeat" denotes that repeat observations were made to calculate errors as described in the text.

were the same as that for the central image. The galaxies observed with grid observations are identified in the notes to Table 1.

2.2. *Image Processing*

The first step in the processing of the images was the subtraction of averaged bias and dark frames. Blank sky frames were generated by combining the dithered sky images taken at each position. Individual sky exposures were multiplicatively scaled to have the same mode and combined by a median to remove the stellar images. An average of the median-combined sky frames from before and after the galaxy image was then constructed for each galaxy observation and subtracted from the individual galaxy frames. On the few occasions in which we did not bracket both sides of a galaxy series, we used the combined sky frame closest in time to the galaxy observation. This first-order sky subtraction did *not* adequately estimate the sky level for precise surface photometry because the brightness of the sky usually showed significant variations on timescales shorter than that between adjacent exposures. This means that the true sky level must be estimated on the galaxy frames themselves; the uncertainty in this estimate of the true sky level is the principal source of error in the surface photometry. We will discuss the method of sky determination below at greater length.

Flat fields were then constructed by averaging all the bias corrected, dark-subtracted, median-combined frames of the sky for each night and scaling this averaged frame to a mean of unity. The processed sky-subtracted galaxy frames were then divided by this flat field. The resulting images were flat to better than 0.1%, as judged by row and column cuts and statistics in image subsets.

The next step was to combine the flattened, sky-subtracted galaxy frames and merge the grid observations of the galaxies. The individual galaxy frames were averaged after shifting in rows and columns to align the position of the galaxy's nucleus as measured by an intensity-weighted centroid in a box of size 15″. This shift-and-align was also applied to each of the frames which made up a grid. The assembly of the grids used the following procedure. Let the intensity in pixel (x, y) of image n be $I_n(x, y)$, $i = 0, 4$ with the image centered on the galaxy nucleus as $I_0(x, y)$. Here (x, y) are coordinates in a global coordinate system such that the nucleus of the galaxy on all frames is $x = 0$, $y = 0$. The image $I_1(x, y)$ was merged with the image $I_0(x, y)$ by first computing via least-squares the coefficients a_1 and b_1 in the intensity transformation

$$I_0(x, y) = I'_1(x, y) \equiv a_1 I_1(x, y) + b_1 , \qquad (1)$$

where all overlapping pixels were included in the least-squares computation. Then the two images were combined by averaging the intensities $I_0(x, y)$ and $I'_1(x, y)$ of overlapping pixels and replicating pixels that did not overlap. After these two images were thus merged to make a proto-grid, the image $I_2(x, y)$ was scaled to match the intensities on the proto-grid via least-squares (yielding coefficients a_2 and b_2) and combined to make a new, larger grid. This process was repeated until all the frames had been merged together. The merger and all subsequent steps in processing and measurement were performed using procedures written for VISTA (Stover 1988). Note that this least-squares procedure brings the several images in a grid to the same sky level as the first image $I_0(x, y)$ by matching the intensities of *all* overlapping pixels. Thus it was not necessary that each image extend far enough away from the nucleus of each galaxy so that the background sky could be measured (see § 2.3).

On nonphotometric nights we determined both a_n and b_n for each image in the grid. On photometric nights, the scaling ratios in equation (1) above were set to $a_n \equiv 1.0$ and only the constants b_n $(n = 1, 4)$ were determined for each image making up the grid. We also experimented with determining a_n on photometric nights; invariably the merger of the individual frames yielded values of a that were within 1% of unity, thus providing a check on the stability of the night on short timescales.

We display gray-scale images of selected galaxies in Figure 1 (Plates 6 and 7). Figure 1*a* shows those observed in a single field, while Figure 1*b* consists of those with grid observations.

2.3. *Determination of the Sky Level*

The most critical step in accurate surface photomery is the determination of the sky level. In CCD observations, one typically measures the sky level on the galaxy frame itself as far away from the nucleus of the galaxy as is practical. In this way one can achieve photometry down to better than 1% of the sky. The traditional approach taken in single-aperture near-IR photometry is to chop at several Hz between object and sky positions. When a two-dimensional array detector is used to image extended objects in the infrared, one cannot sample the sky level as fast as the timescale for significant (here greater than 1%) variations. We illustrate this in Figure 2, where we plot the mean intensity of all the galaxy and sky frames for observations on UT 1990 October 19 (a photometric night). Shown as open circles are the mean intensity of the average sky frames; plusses are the mean intensity on the individual galaxy frames, which includes the level of the sky plus the light contributed by the galaxies themselves. The right axis in Figure 2 shows the intensity in counts on a logarithmic scale, while the left axis shows the level in K mag arcsec^{-2}, computed from the counts via the photometric transformation appropriate for that night. The horizontal axis is in hours after UT midnight. This figure shows that the long-term variations in the sky level can be quite large ($\pm 20\%$), and that changes of several percent

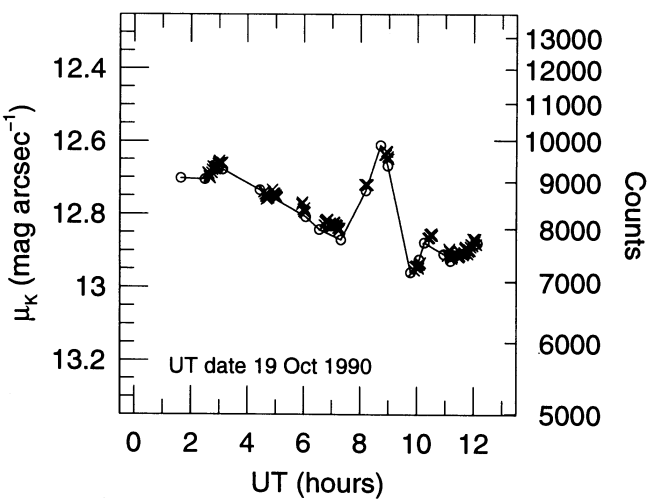

FIG. 2.—Intensity of the sky during one night of observations, shown as a function of hours after UT midnight on 1990 October 19. The open circles connected by a solid line and the crosses, respectively, show the intensity of the sky and galaxy frames in the sky/object/sky observations. See the text for more details.

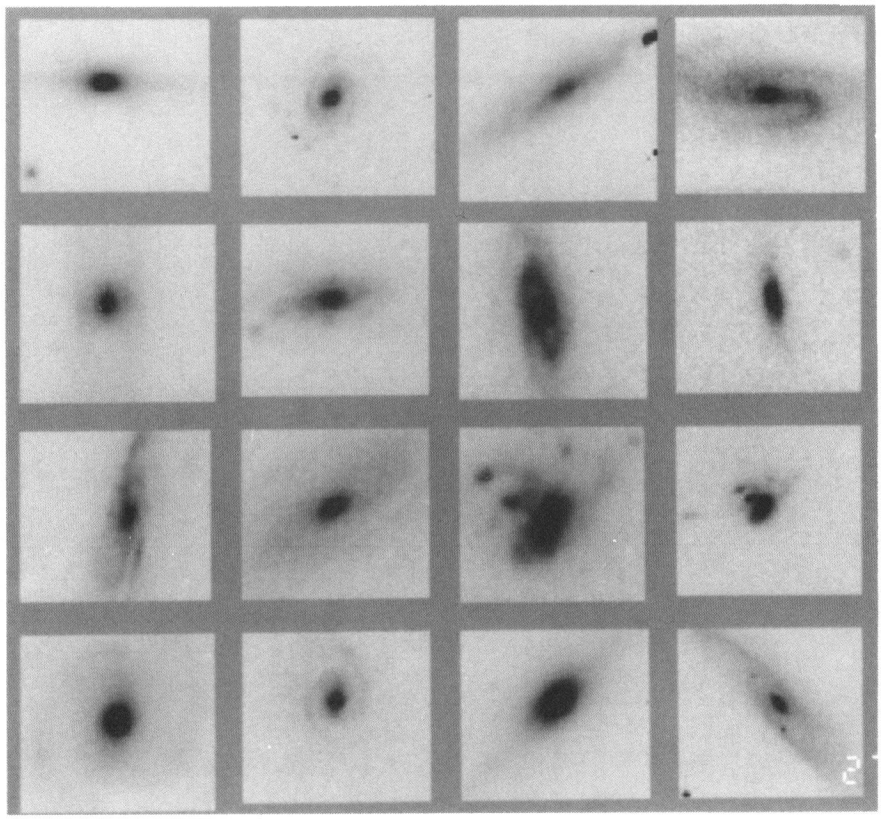

FIG. 1*a*

FIG. 1.—(*a*) Selected images from the survey. From left to right, the galaxies in this figure are (*top row*): NGC 128 (1.3 m telescope, *J* filter), NGC 753 (1.3 m, *K*), NGC 1035 (1.3 m, *K*), and NGC 3672 (1.3 m, *K*); (*second row*): NGC 4448 (1.3 m, *K*), NGC 7448 (1.3 m, *J*), NGC 7537 (2.1 m, *K*), and NGC 7537 (1.3 m, *K*); (*third row*): NGC 7541 (1.3 m, *K*), NGC 7606 (1.3 m, *K*), NGC 7673 (2.1 m, *J*), and NGC 7673 (1.3 m, *K*); (*bottom row*): NGC 7798 (2.1 m, *J*), NGC 7798 (1.3 m, *K*), NGC 7814 (1.3 m, *K*), and NGC 7817 (1.3 m, *K*). In this figure, north is to the left and east is up. (*b*) Selected grid observations, all obtained on the 1.3 m telescope. From left to right the galaxies are (*top row*): NGC 697 (*K*), NGC 891 (*J*), and NGC 891 (*K*); (*center row*): NGC 1175 (*K*), NGC 4565 (*J*), and NGC 4565 (*K*); (*bottom row*): NGC 5033 (*J*), NGC 7331 (*J*), and NGC 7332 (*K*). Orientation of the galaxies is as in Fig. 1*a*.

PLATE 7

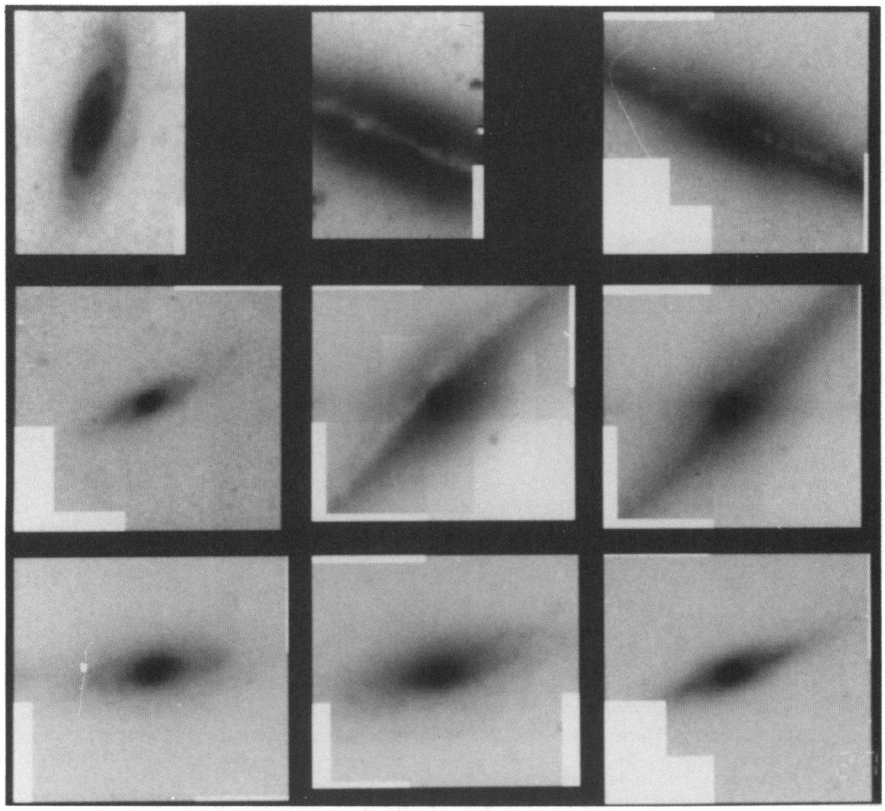

FIG. 1*b*

TERNDRUP et al. (see 432, 520)

can take place in intervals of a few minutes. The short-term variations can be gauged by the dispersion in the mean level of the individual galaxy frames or by the dispersion in the additive constants applied in merging the sky frames or constructing image grids. The dispersion was typically 15–45 counts (0.2%–0.6% of the sky) over periods of a few minutes, and up to 100–200 counts (1.3%–2.6% of the sky) over the length of time it took to image all the frames that constituted a grid of observations on the large galaxies. Long-term variations in the J and H bands are usually significantly larger; the sky level at these wavelengths can change by as much as a factor of 1.5 to 2 in the course of a night.

The sky levels shown in Figure 2 were among the brightest during our observing runs, with the largest long-term variations. For the other nights, the mean sky level at K was $\mu_K = 13.0 \pm 0.3$ (s.d.) mag arcsec^{-1} with long-term changes of 10%–15% throughout each night. The short-term variations in the sky levels for any night were similar to that shown in Figure 2.

Even the short-term variations are significant compared to the surface brightness of most of the galaxies in our sample. We illustrate this by considering NGC 7331, which has a relatively high central surface brightness of $\mu_K = 12.72 \pm 0.02$ mag arcsec^{-2}; as is typical, the galaxy contributes only a few percent of the light on the frame. The average sky level immediately before and after the galaxy (grid) observations was $\mu_K = 12.85$ and 12.73 mag arcsec^{-2}, respectively, a difference of 6%. The sky frames on either side of the galaxy grid were the average of four exposures of 90 s. The short-term variation (as measured by the dispersion) in the sky brightness on both sets of four frames was 1.5%. The major-axis profile of NGC 7331 falls to 6% of the sky at a major-axis distance of only $a = 16''$; it reaches a level of 1.5% of the sky at $a = 55''$. Therefore, it is necessary to determine the true sky value from the galaxy frame itself to remove the effects of short-term sky brightness variations.

On the sky-subtracted galaxy frames, we determined the modal background value in 3 to 5 regions located as far from the nucleus as possible, in practice along the minor axis of the galaxy. We then took the average of these values as the sky correction and subtracted this average from the galaxy frames. The dispersion in the background sky level in different parts of the frames was almost always less than 0.5% of the mean sky level, averaging 0.21% of the sky. We normally set the error in the sky to be the dispersion in the background level; in those cases where the dispersion was comparable to our estimated error in the flat fielding (0.1% of sky, above § 2.2), we set the error in the sky to be 0.15% of the sky level. For the grid observations, the sky was measured as for the single-field frames (i.e., from the average value in regions far from the nucleus) after the grid was assembled.

The determination of the sky level on the 2.1 m frames was problematic, because in nearly all cases the galaxy filled the frame. We therefore chose to use the 1.3 m data both to determine the sky level and set the photometric zero point for the 2.1 m data. The method was to match the major-axis brightness profiles $\mu_{1.3}(a)$ and $\mu_{2.1}(a)$ from the 1.3 and 2.1 m, respectively, according to

$$\mu_{1.3}(a) = -2.5 \log [\Sigma_{2.1}(a) - s] + \mu_0 , \quad (2)$$

where a is the major-axis length of the profiles, the μ terms are magnitudes, and $\Sigma(a)$ is the brightness along the major-axis profiles in counts. The sky level s and the zero-point μ_0 were determined via least squares over a range in semimajor axis $5'' < a < a_{\max}$, where $a_{\max}$ was the maximum extent of the 2.1 m profiles. (The measurement of these profiles is discussed below.) The 2.1 m profiles were interpolated in radius to the 1.3 m points for the least-squares fitting; the constants s and μ_0 were then applied to the uninterpolated 2.1 m instrumental magnitudes. When there were both J and K observations on the 1.3 m, the 2.1 m profiles in each color were independently calibrated. In cases where J observations were made on the 2.1 m but not on the 1.3 m they could not be treated in this way and thus were not used in the following analysis.

2.4. *Photometric Calibration*

The 1.3 m galaxy observations made on photometric nights are denoted with an "s" in column (8) of Table 1. Standard stars from the list of Elias et al. (1982) were observed at a large range of air mass. Transformations of the form

$$K = k + c_{k,1} X + c_{k,2} ,$$
$$J - K = c_{jk,0}(j - k) + c_{jk,1} X + c_{jk,2} , \quad (3)$$

were sufficient, in most cases, to bring each night's observations onto the CTIO/CIT system with residuals in K or $J-K$ of 0.02 mag or less; here X is the air mass, J and K are magnitudes on the standard system, and the instrumental magnitudes j and k are defined as $-2.5 \log_{10}$ (counts s^{-1}), where the counts were measured in an aperture of diameter 9.″5.

The color transformation coefficient was determined from the average value for all photometric nights to be $c_{jk,0} = 0.960 \pm 0.003$ (s.d.). The coefficients for the air mass terms and the zero points were determined independently for each night. The solution for one night required a small term in UT since the transparency improved by 0.03 mag during the night. Figure 3 plots the residuals in K and $J-K$ from equation (3) for all the photometric nights as a function of $J-K$. The errors in a single measurement of a standard star were estimated from the scatter after the transformation and are $\sigma_K = 0.013$ and $\sigma_{J-K} = 0.025$.

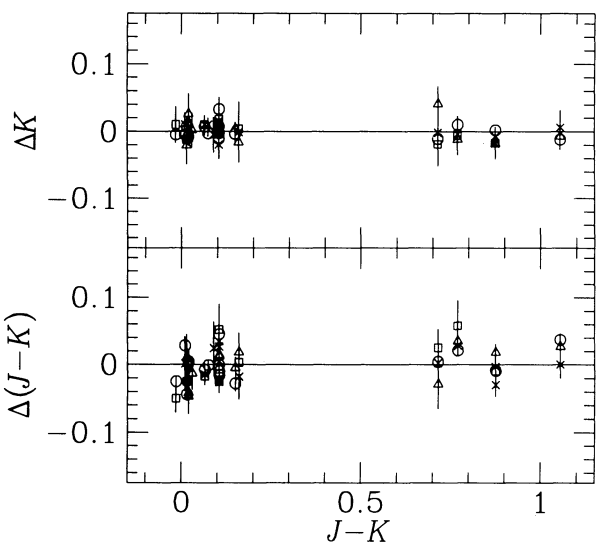

FIG. 3.—Residuals in the transformation to the CTIO-CIT photometric system, in the sense observed *minus* catalog value as a function of catalog $J-K$. The different symbols represent residuals on the four nights of the observing runs for this project that were photometric.

Intermittent thin cirrus was usually responsible for nonphotometric conditions. Some of the images from these nights could be calibrated via published aperture photometry as described in the next section. For those galaxies without previously published aperture photometry, we transformed the surface brightness to magnitudes and computed colors assuming that the night was transparent with the average solutions for photometric nights of the same run. Based on repeated observations of the same object on these nights we estimate that the absolute level of the photometry in both K and J can be in error by a few tenths of a magnitude, uncertainties in the $J-K$ color will be less. These galaxies are given the designation "n" in column (8) of Table 1.

2.5. *Comparison to Aperture Photometry*

As a check on our method of photometric calibration and to generate photometric calibrations for some galaxies observed under nonphotometric conditions, we computed instrumental synthetic aperture magnitudes according to

$$m(d) = -2.5 \log [\sum I(x, y)] , \quad (4)$$

where d is the diameter of an aperture centered on a galaxy nucleus; the sum was carried out over all pixels with central position less than or equal to a distance $a = d/2$ from the galaxy's nucleus. We then compared the synthetic aperture magnitudes for those galaxies observed on photometric nights to those published in the literature by computing the magnitudes $j(d_n)$ and $k(d_n)$ for each aperture d_n, and transforming these to the CTIO/CIT system via the appropriate photometric solution.

Figure 4 shows the differences between our synthetic aperture magnitudes and those in the literature for all galaxies with previously published photometry. No attempt has been made to transform the published photometry from other systems to the CTIO/CIT system. For apertures larger than $d > 10''$, the agreement between the synthetic and published values is good:

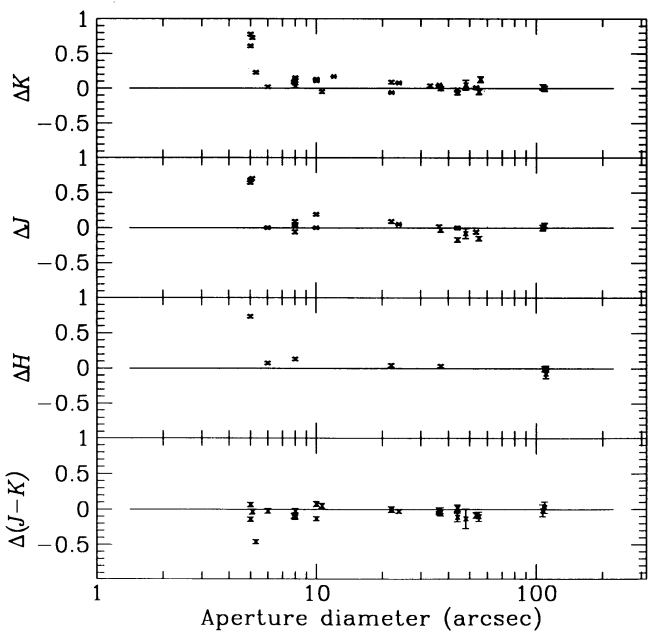

FIG. 4.—Differences between synthetic aperture magnitudes and colors computed from the data in this paper and aperture photometry found in the literature. The differences are plotted as a function of aperture diameter.

the mean differences (in the sense ours *minus* published) and standard deviations are J: -0.008 ± 0.095; H: -0.007 ± 0.042; and K: $+0.035 \pm 0.069$. If we compare our results to photometry that we consider especially reliable and which are on the CTIO/CIT standard system (Frogel et al. 1978; Aaronson 1979; Aaronson et al. 1980, 1982; Bothun et al. 1985), the scatter is smaller: the mean difference and standard deviations are $+0.002 \pm 0.048$, -0.006 ± 0.026, and $+0.016 \pm 0.042$ mag in J, H, and K, respectively. This scatter is approximately what is expected from the errors in the aperture photometry, typically quoted as 0.01–0.02 mag, and the errors in our synthetic apertures, which are 0.02 mag at small radii, increasing to 0.04 mag for $d > 45''$. The excellent agreement between the large aperture single channel measurements and our surface photometry confirms the accuracy of our sky determinations and photometric calibration.

2.6. *Profile Fitting*

We used the routine PROFILE (Lauer 1985) in VISTA to measure the surface brightness of our galaxies. Each galaxy was modeled as a series of concentric ellipses, yielding for each semi-major axis length a the average surface brightness $\Sigma(a)$ of the best-fitting ellipse, the position angle θ, and ellipticity $\epsilon(a) \equiv 1 - b/a$, where b is the length of the semi-minor axis. Before measurement, dead pixels and the images of nearby stars were eliminated by replacing intensities significantly higher or lower than a local modal value with the mode. The interval between adjacent values of a was taken as 1 pixel. The routine also determined azimuthal intensity deviations which measure the boxiness of the isophotes (Lauer 1985; Jedrzejewski 1987; Franx, Illingworth, & Heckman 1989; Peletier et al. 1990). The analysis of the isophote shapes and residuals from the fits to the ellipses will be discussed in a later paper.

Isophotes were fit out to the radius at which the galaxy's major axis ran into the edge of the frame, or when we could no longer discern via contour plots or intensity stretches on displays that there was any significant galaxy light. Major-axis profiles in K (and in $J-K$, when available) were constructed by taking $\Sigma(a)$ for each value of a and transforming these to mag arcsec^{-2} using the photometric calibrations discussed above. Because the position angle θ may vary with major-axis length a, the major-axis profiles measured in this way will not be the same thing as a cut along the bulge or disk. This method, besides being easy to implement, has the advantage that it is identical to the approach followed by Kent (1984, 1986, 1987), thus facilitating comparison to his photometry. We constructed profiles in $r-K$ by taking Kent's major-axis profiles and linearly interpolating his values of surface brightness onto our sampled radii.

The ellipse-fitting program estimates an error $\sigma_{\rm phot}$ in $\Sigma(a)$ from photon statistics on the galaxy and background sky level. For most of the galaxies, $\sigma_{\rm phot} \leq 0.05\Sigma$ in the core, and increases to several tenths mag at large radii. We found from experimentation that the contour fitting program was able to determine the brightness profiles out to the radius at which $\sigma_{\rm phot} \approx 0.5\Sigma$, beyond which it often converged to profiles that had ϵ or θ which were significantly different from those fit at smaller radii. In addition, there is the uncertainty in the sky level $\sigma_{\rm sky}$ which was determined as discussed above (§ 2.3). Except for a few galaxies with very low central surface brightness, $\sigma_{\rm phot} < \sigma_{\rm sky}$ for $a < 30''$. We estimated a total error according to $\sigma_{\rm tot} = (\sigma^2_{\rm phot} + \sigma^2_{\rm sky})^{1/2}$ for K. For $J-K$ we computed $\sigma_{\rm tot}$ for J and combined it with the K error in quadra-

ture. We assumed that the errors in Kent's r-band photometry were smaller than those in K, and set $\sigma_{tot}(r-K)=\sigma_{tot}(K)$. The final error estimate does not include the absolute photometric errors, which (§ 2.4) are $\sigma_K=0.013$ and $\sigma_{J-K}=0.025$.

The surface photometry for our galaxies is displayed in Figure 5. Data for an individual galaxy are arranged from top to bottom and are plotted as a function of semimajor axis length a. The scale along the bottom axis shows the values of a in arcsec, while the scale on the top shows the projected major-axis distance in each galaxy in kpc, calculated directly from the Virgo infall-corrected radial velocity tabulated in de Vaucouleurs et al. (1991), assuming $H_0=75$ km s^{-1} Mpc^{-1}. The upper three panels show (reading down from the top) $\mu_K(a)$, $J-K$ color, and $r-K$, respectively. Data from the 1.3 m telescope are shown in these three panels as plusses; the open circles show the 2.1 m data calibrated as described above. The K surface brightness and colors are plotted out to the radius at which $\sigma_{tot}(K)=0.25$ mag; at this radius the error in $J-K$ is typically about 0.3 mag. For those galaxies observed on nights with high sky brightness (§ 2.3), the limiting magnitude at which $\sigma_{tot}(K)=0.25$ mag is about $\mu_K=17.8$; for those galaxies observed under the best conditions the limit of the photometry is about 1 mag fainter. The central surface brightness, which represents the average intensity over the innermost pixel, is plotted at a radius of $a_0/2^{1/2}$, where a_0 is the size of one pixel, 0.″54 and 1.″35 on the 2.1 and 1.3 m, respectively.

The lower two panels show the ellipticity of the fitted isotopes and the position angle of the isophotes measured from north ($\theta=0°$) through east ($\theta=90°$). These panels show only the 1.3 m data, with plusses denoting the K data, and crosses for the J results. Here, the points extend to the full radius to which isophotes were fit, regardless of error. In virtually all cases, the ellipticities and position angles are nearly identical in both J and K. To illustrate this last point, we show (Fig. 6) the differences in ϵ and θ between observations at K and at J. This figure shows that even for round isophotes ($\epsilon<0.2$), there is good agreement between the independent J- and K-values, though with somewhat larger scatter than for more elongated isophotes.

As a partial check on our methods, observations of several galaxies were repeated NGC 474 and NGC 670 were re-observed on the 1.3 m in K on more than one photometric night and independently calibrated. We also have analyzed a K image of NGC 7469 obtained on the 2.5 m duPont telescope at Las Campanas. This image has a total on-galaxy exposure of 800 s at a spatial scale of 0.″35 pixel^{-1} and was obtained with a 256 × 256 HgCdTe detector with a field size of 91″, about 12% larger in radial extent than the field of the KPNO 1.3 m observations. For these repeat observations, Figure 7 displays (*top to bottom*) the differences in major-axis profiles, ellipticity, and position angle, respectively. The profile for the uncalibrated Las Campanas observations of NGC 7469 was adjusted to match the photometry for this galaxy measured at KPNO over $a<20''$. The mean difference in the profiles for NGC 474 (*left panel*) and for NGC 670 (*center*) are −0.002 mag and −0.010 mag, respectively, well within our estimates of the error in the photometric calibration. The dispersion in ellipticity and position angle for all three galaxies together ($a<20''$) is 0.025 and 3.5 degrees, respectively.

3. BULGE AND DISK COLORS

We now examine the major-axis profiles which are presented in Figure 5, and discuss a simple determination of the mean colors and color gradients in regions of the profiles that are dominated by the disk or the bulge. In this analysis we overlook many of the complexities of the profiles. For example a comparison of the images of the galaxies in Figures 1*a* and 1*b* with the surface brightness profiles in Figure 5 shows several instances of arms or other structures which appear as bumps in the μ_K profiles. Examples are NGC 697, 753, 3672, 5033, 7448, 7537, 7541, 7606, and 7817. In several cases corresponding features are also evident in the $J-K$ and $r-K$ color plots as well. In a subsequent paper we will discuss a full decomposition of the major-axis J and K band profiles and the two-dimensional structure of the galaxies including a harmonic analysis of the isophote shapes.

3.1. *Derivation of the Colors*

Our analysis of the colors began with an inspection of the profiles of surface brightness, ellipticity, and position angles in Figure 5. We estimated a radius a_b for each galaxy inside of which the contribution from the bulge contributes most of the light in the K surface brightness profile, and a radius a_d outside of which the bulge contribution is negligible. The quantities a_b and a_d are given in columns (2) and (3) of Table 2. Generally $a_d\neq a_b$ because there is a transition zone where the bulge and disk both contribute to the profile. The evidence for a bulge contribution was either that the K surface brightness profile at small radii was brighter than an exponential trend exhibited by the profiles at large radii, or that the isophotes were rounder at small radii than at large. For the galaxies of type Sb or earlier, the central surface brightness of the bulge was more than 1.5 mag brighter than the (exponential) profile disk extrapolated to $a=0$, so we estimate that more than 60% of the light within a_b is from the bulge. For later-type galaxies, of course, this fraction is smaller.

The earliest Hubble types in our sample, e.g., NGC 474, NGC 1023, and NGC 7457, exhibit a power-law decline indicating that the luminosity of the region we observed is dominated by a bulge component; later Hubble types, e.g., NGC 1620, NGC 2654, and NGC 3672, show a prominent shoulder or shoulders at intermediate radii in their luminosity profiles accompanied by a rapid increase in ellipticity outward indicating the presence of a disk. Yet later Hubble types, e.g., NGC 801 and NGC 7537, consist almost entirely of a disk component and are highly flattened at all radii, the bulge being essentially absent.

With one exception, the sizes of the bulge components given in Table 2 are $\lesssim 10''$. Griesmith et al. (1982) compared integrated bulge and disk colors by measuring the colors within a standard aperture size of $\log(A/D_0)=-0.86$ to the colors in larger apertures; Aaronson (1979) used $\log(A/D_0)=-0.6$. We computed values of $\log(A/D_0)$ for the bulge-dominated regions of the major axis profiles by setting $A=a_b$ and taking D_0-values from the RC3. We find that $\log(a_b/D_0)<-1.5$ for three-quarters of the sample and $\log(a_b/D_0)<-1.0$ for the remainder, considerably smaller than the apertures employed by Aaronson or by Griersmith et al. Their bulge colors must therefore contain a larger contribution from disk light than do ours. Thus our separation of the profiles into disk- and bulge-dominated regions yields for the first time measures of near-IR colors at radii where it is established that the bulge surface brightness dominates over that of the disk.

Bulge and disk colors were estimated by inspection of Figure 5; bulge colors refer to the mean color of the major-axis profile measured from the innermost sampled radius out to a_b, while

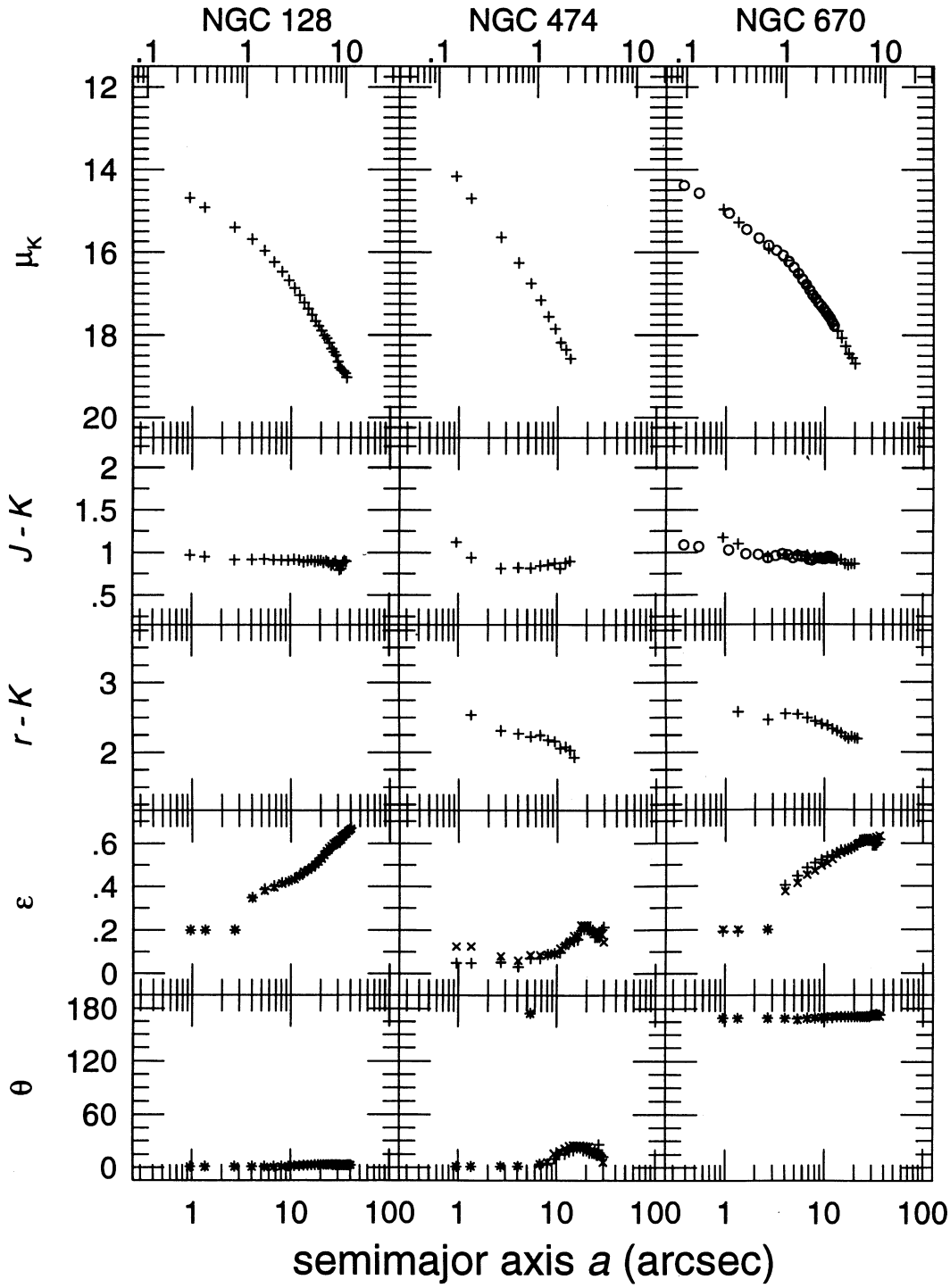

FIG. 5.—Presentation of the surface photometry. Data for an individual galaxy are arranged from top to bottom and are plotted as a function of semi-major axis length a. The scale along the bottom axis shows the values of a in arcsec, while the scale on the top shows the projected major-axis distance in each galaxy in kpc, calculated from the radial velocity assuming $H_0 = 75$ km s^{-1} Mpc^{-1}. The upper three panels show (reading down from the top): K surface brightness in mag arcsec^{-2}; the $J-K$ color; the $r-K$ color, where r is the Gunn-Thuan magnitude from Kent (1984, 1986, 1987). Symbols in the top three panels are: *plusses*, 1.3 m data; *open circles*: 2.1 m data. The lower two panels show ellipticity of the fitted isotopes and position angle of the isophotes measured from north through east. In these panels plusses denote the K data, while crosses are for the J observations. An asterisk (*) next to a galaxy's name indicates that the data were obtained under slightly nonphotometric conditions.

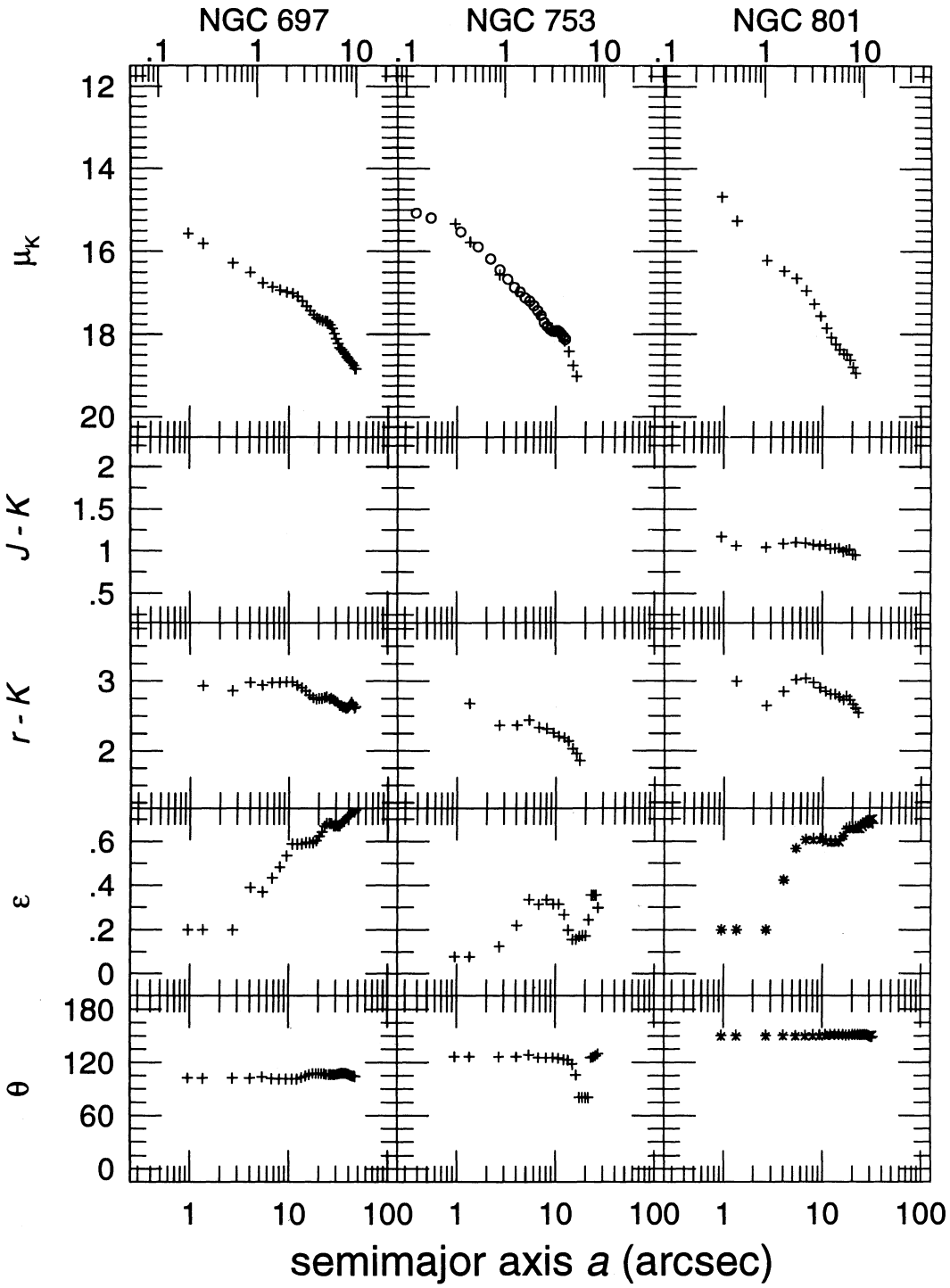

FIG. 5—*Continued*

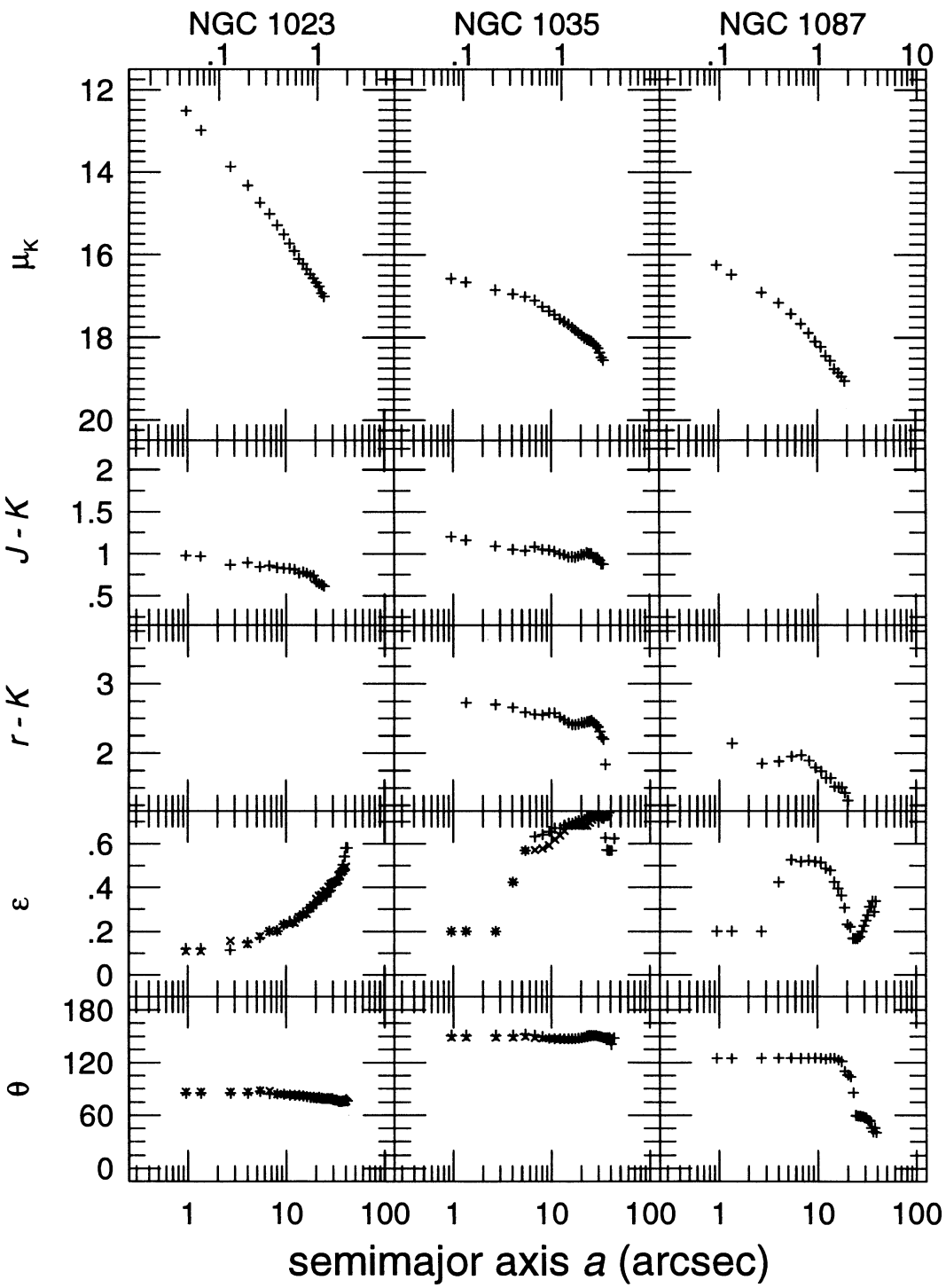

FIG. 5—*Continued*

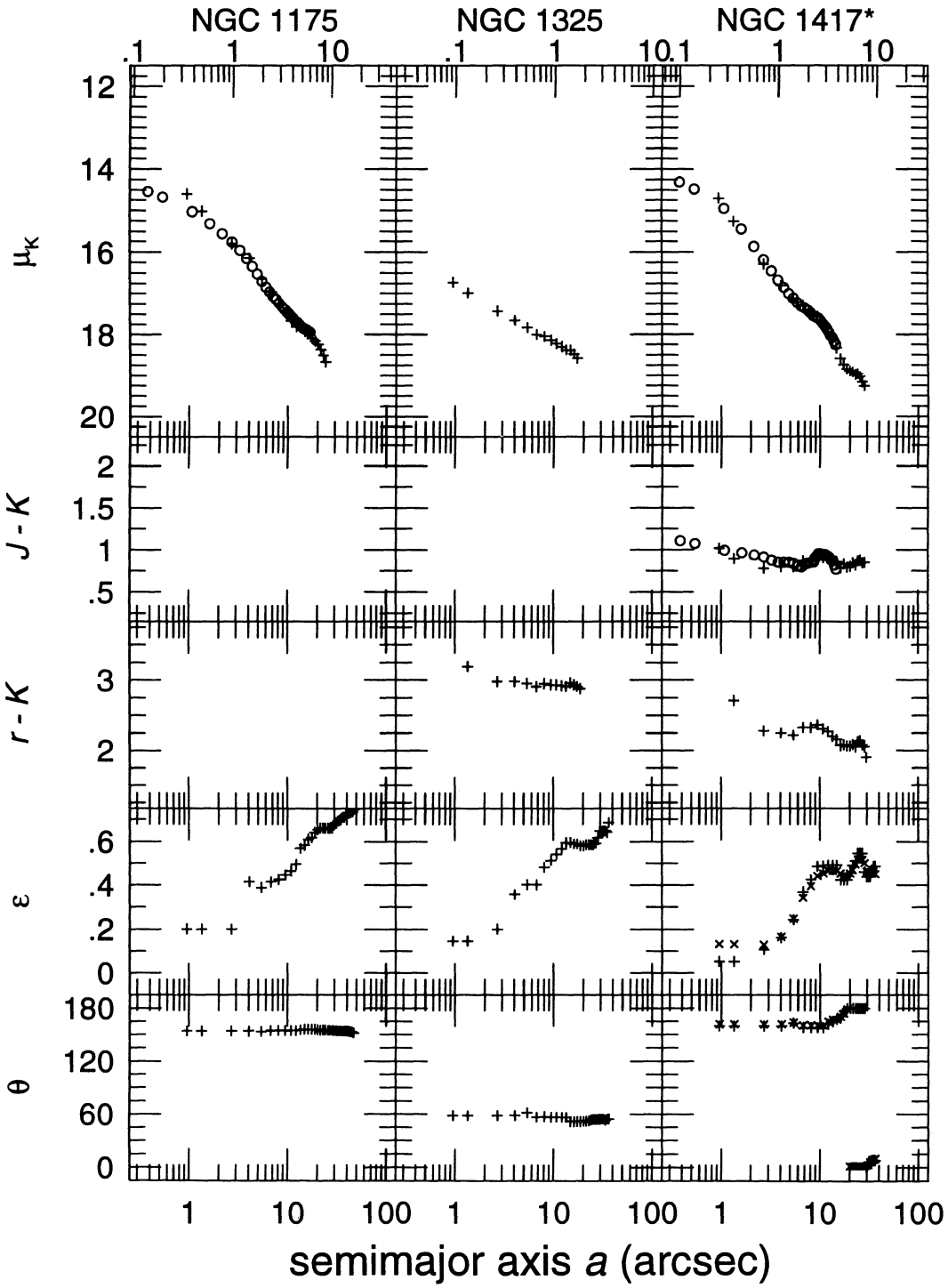

FIG. 5—*Continued*

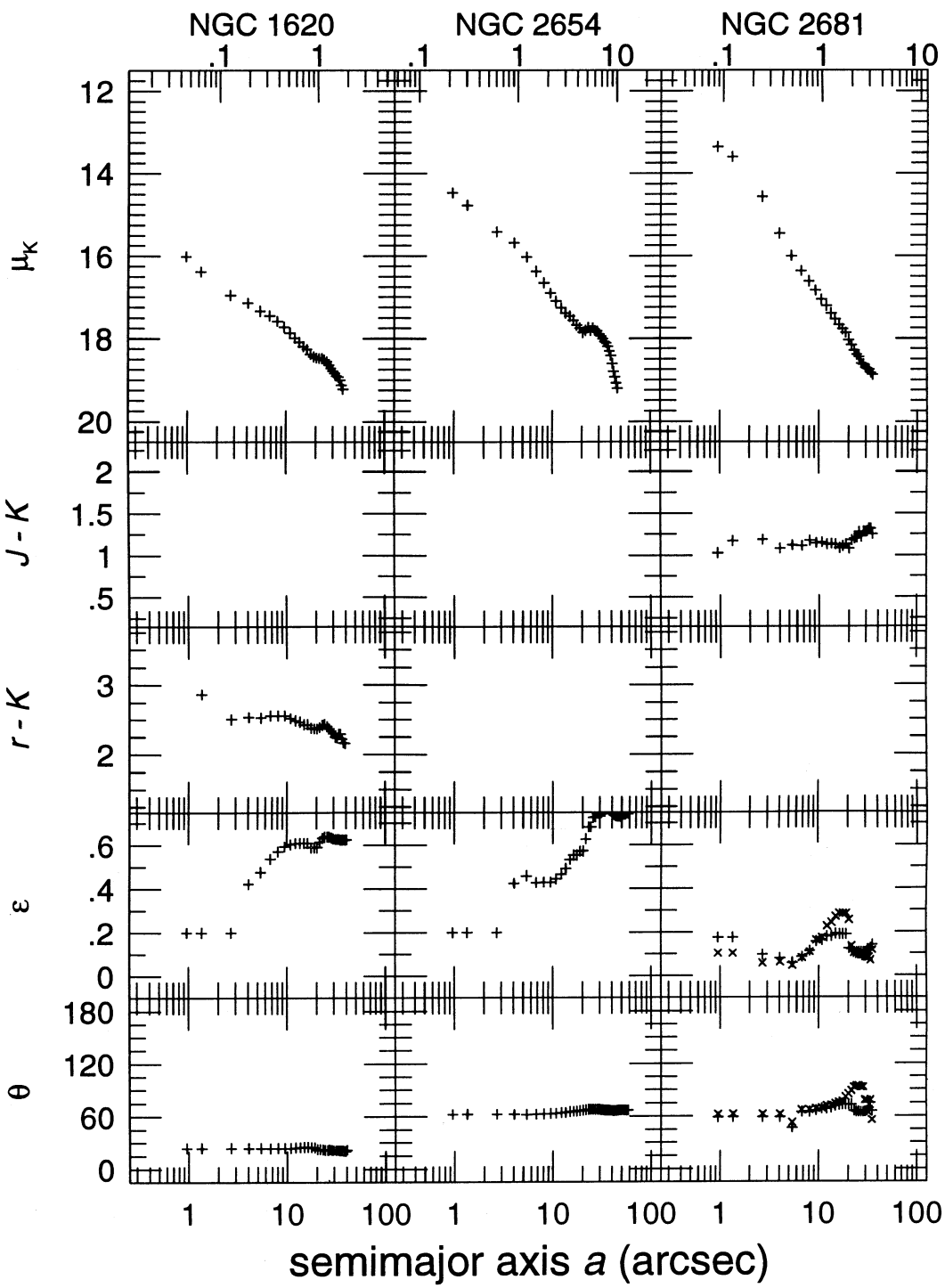

FIG. 5—*Continued*

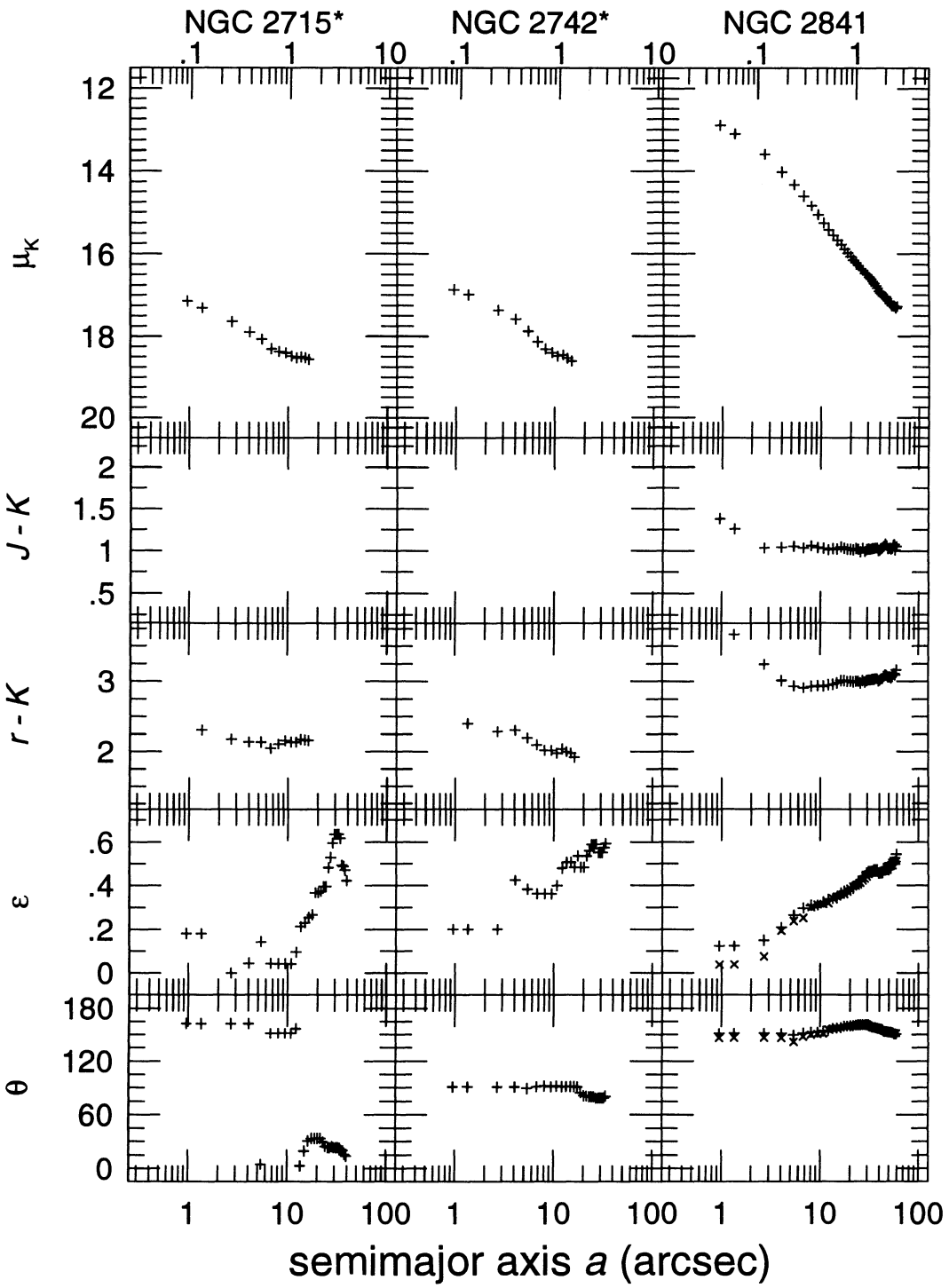

FIG. 5—*Continued*

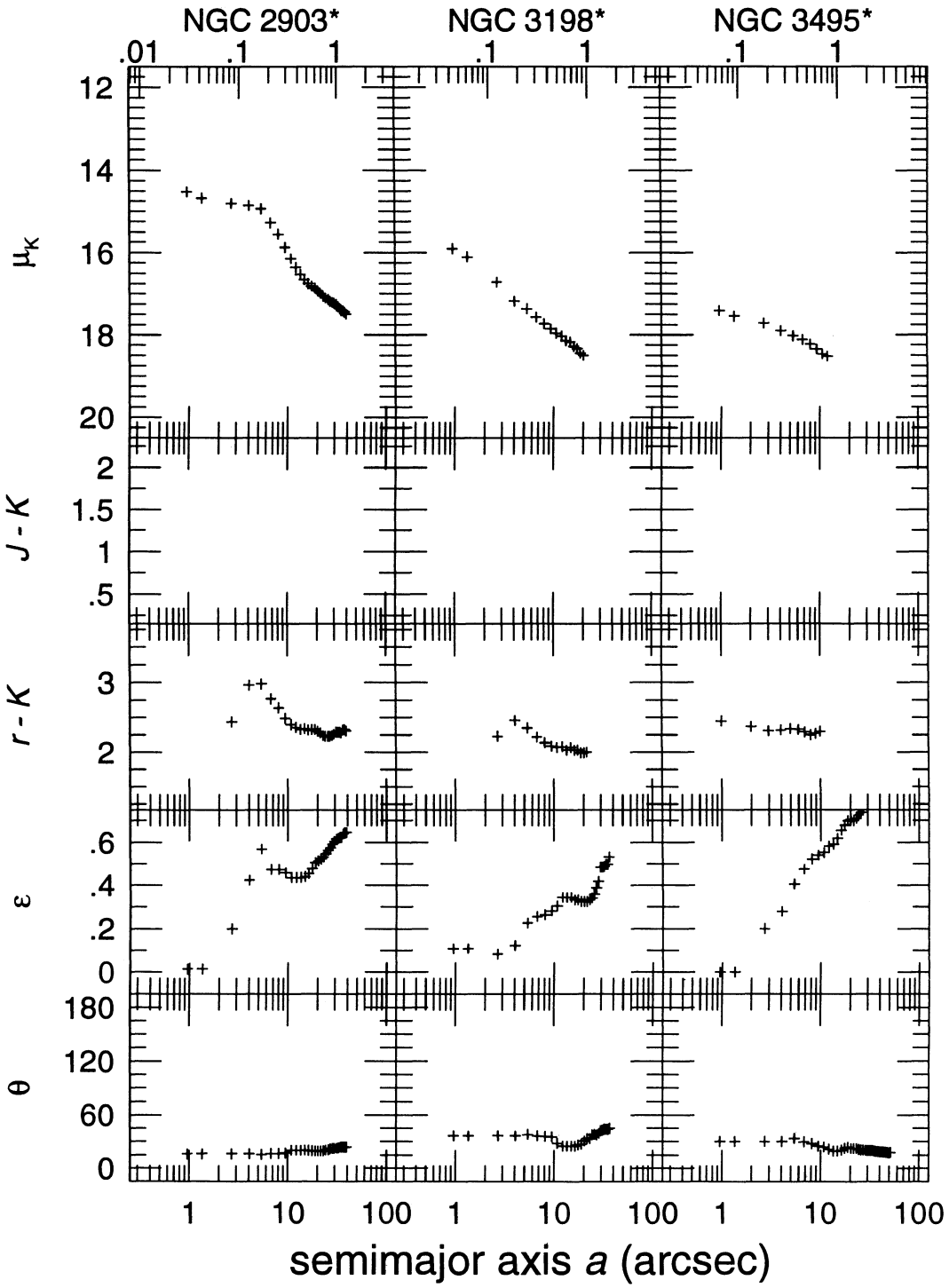

FIG. 5—*Continued*

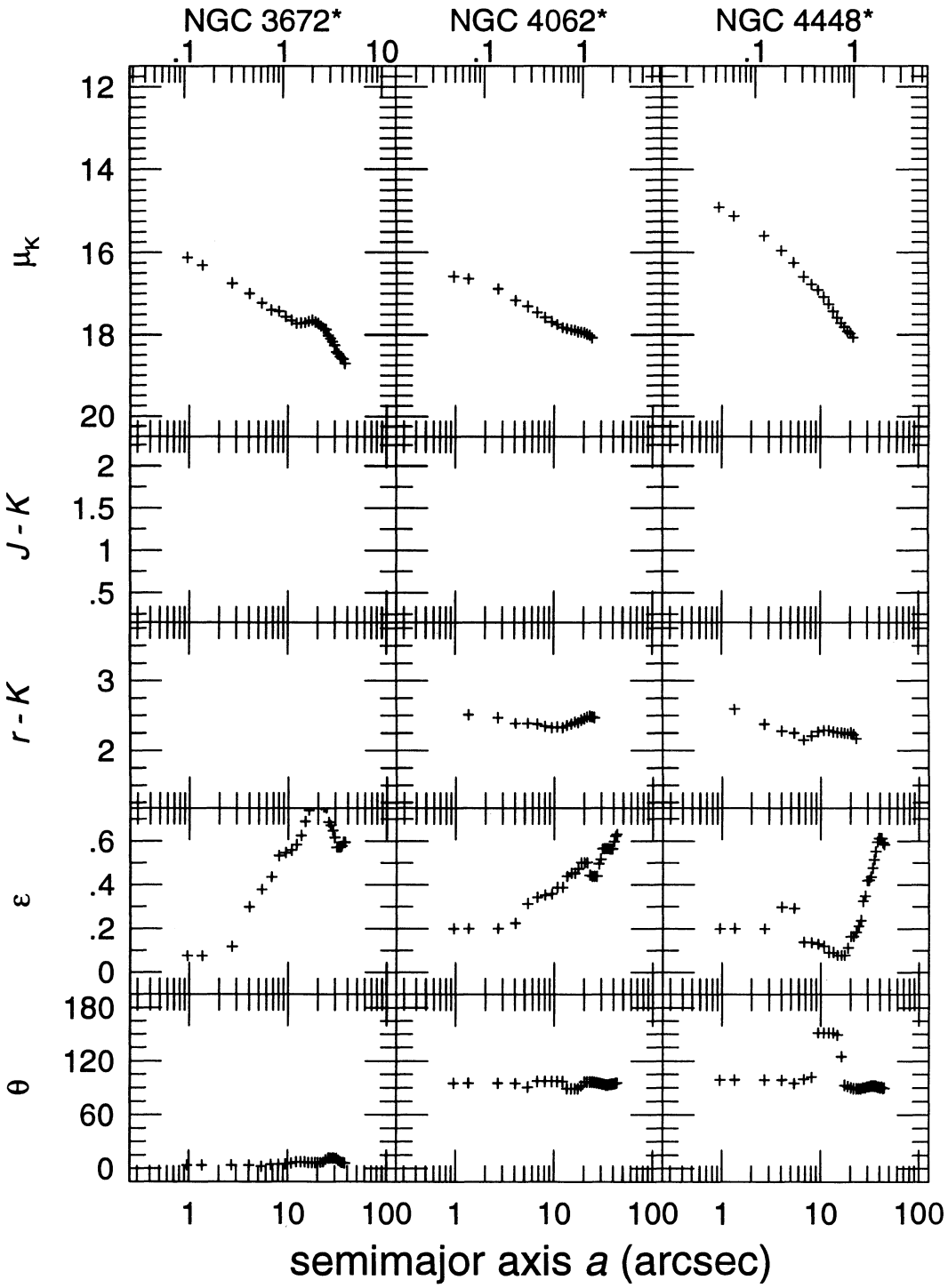

FIG. 5—*Continued*

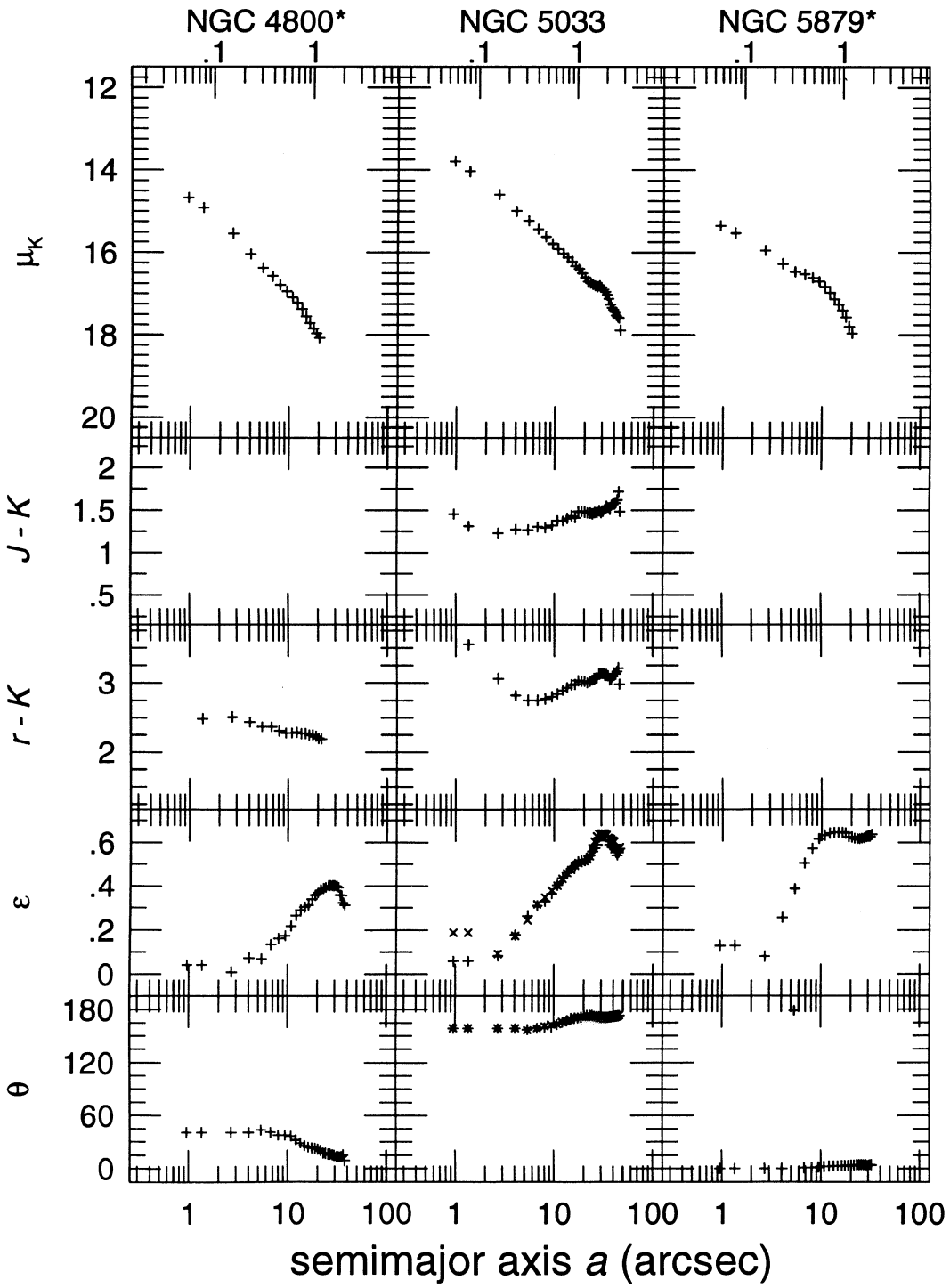

FIG. 5—*Continued*

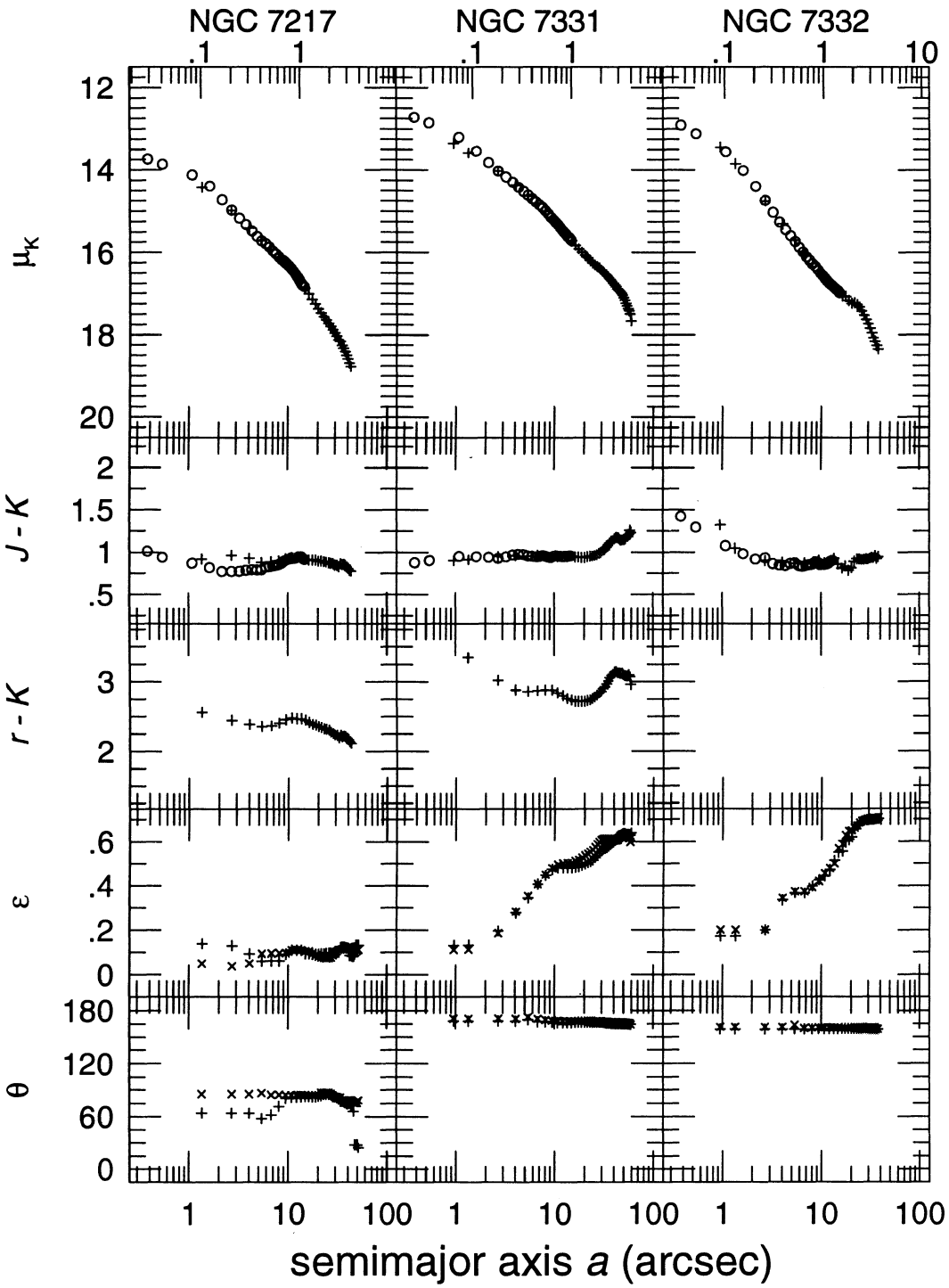

FIG. 5—*Continued*

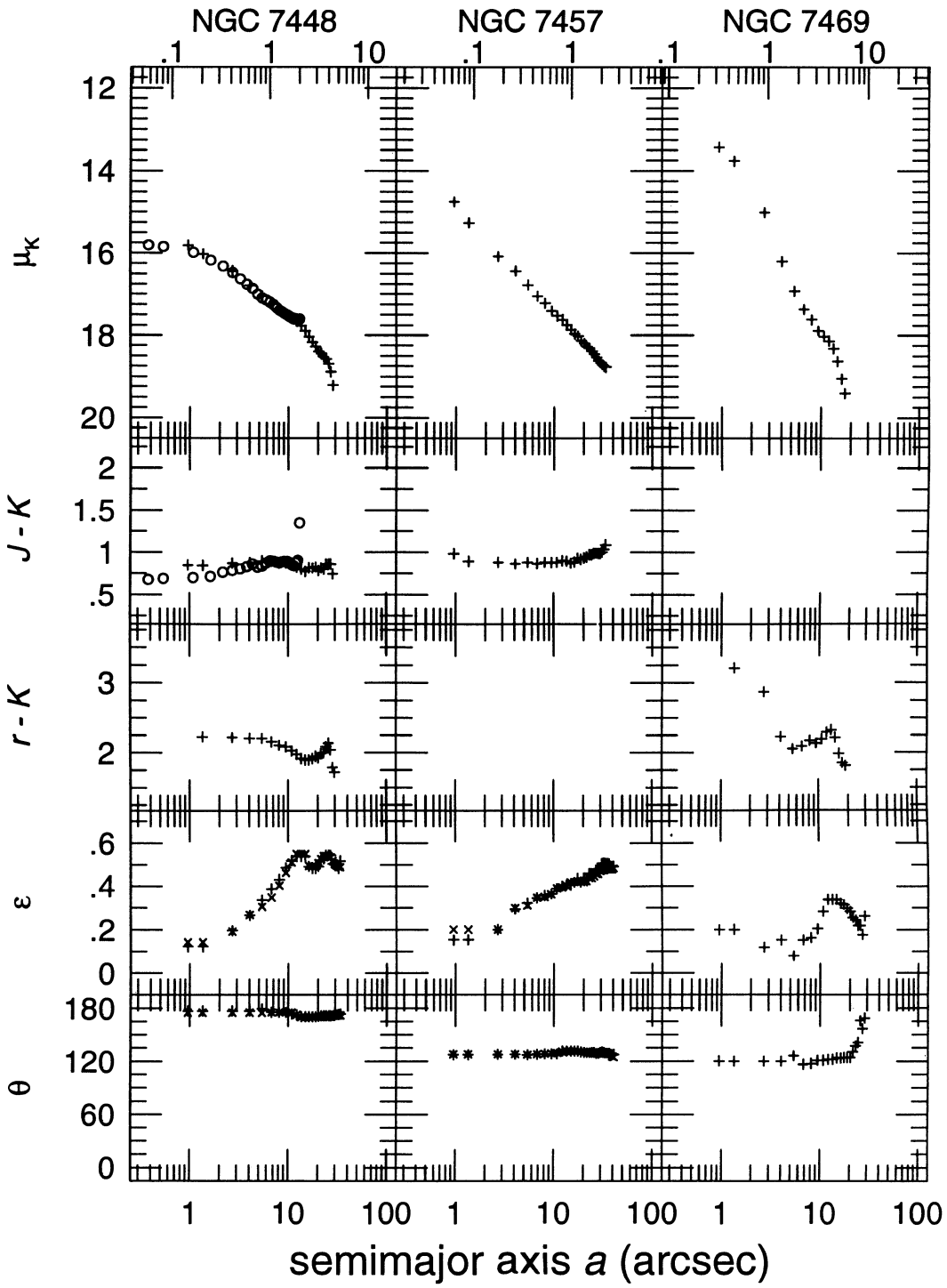

FIG. 5—*Continued*

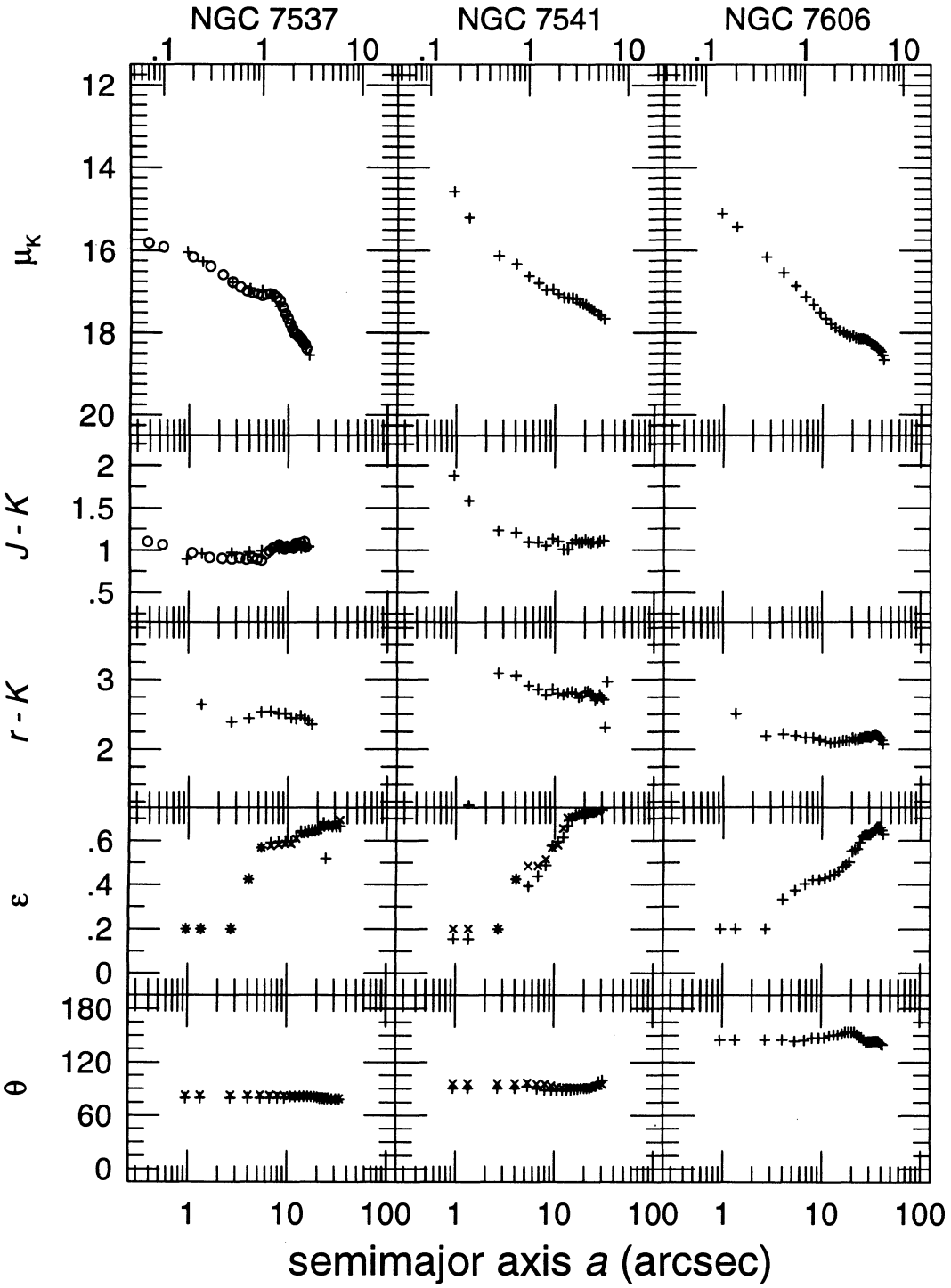

FIG. 5—*Continued*

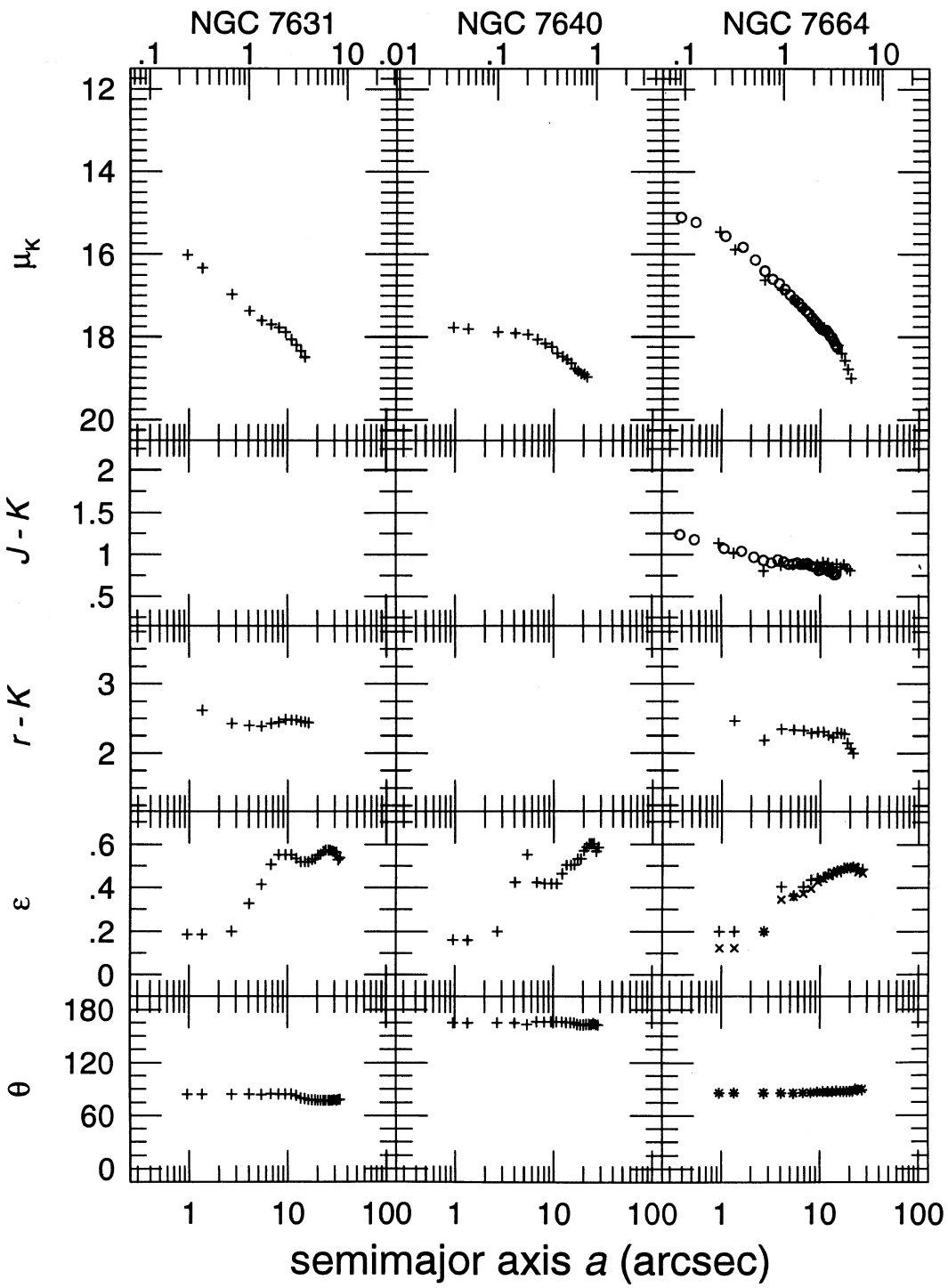

FIG. 5—*Continued*

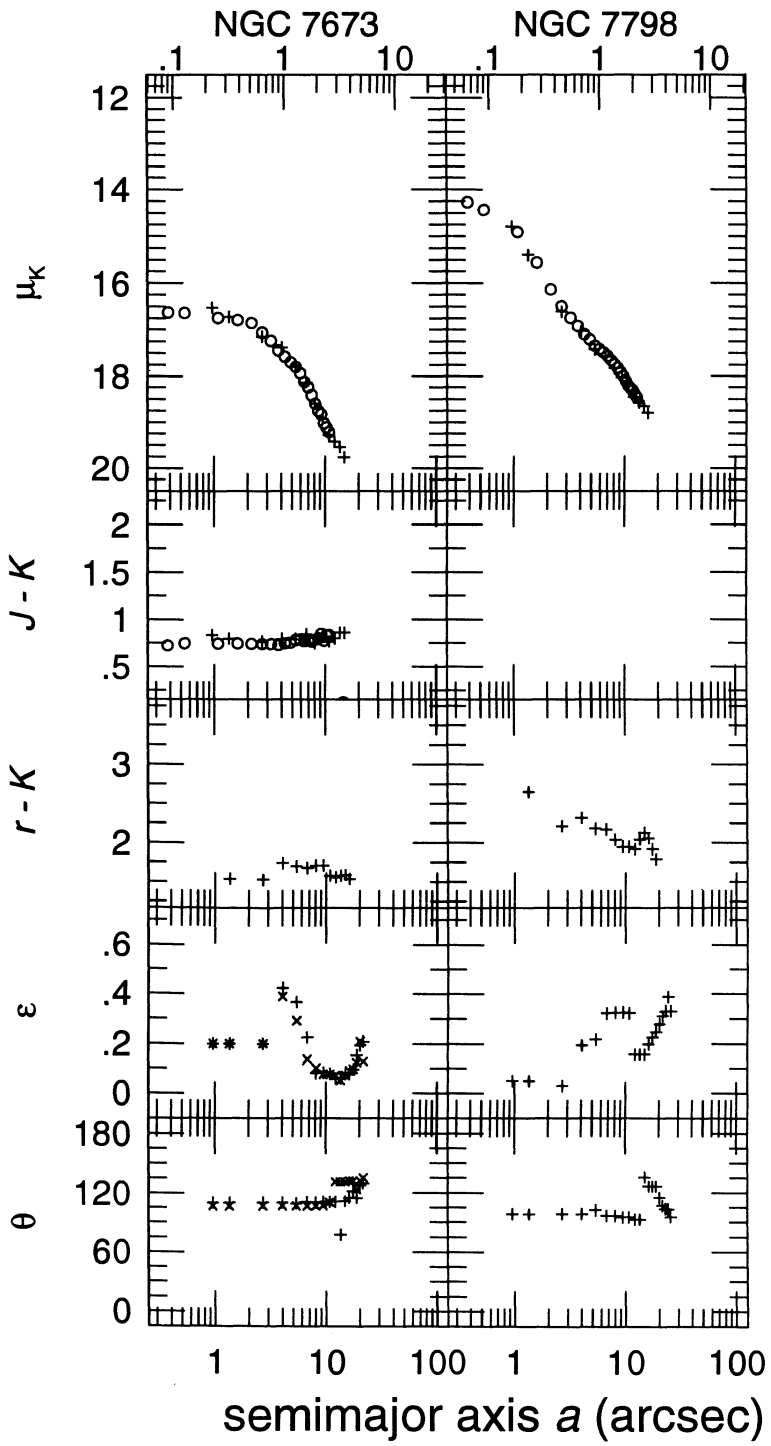

FIG. 5—*Continued*

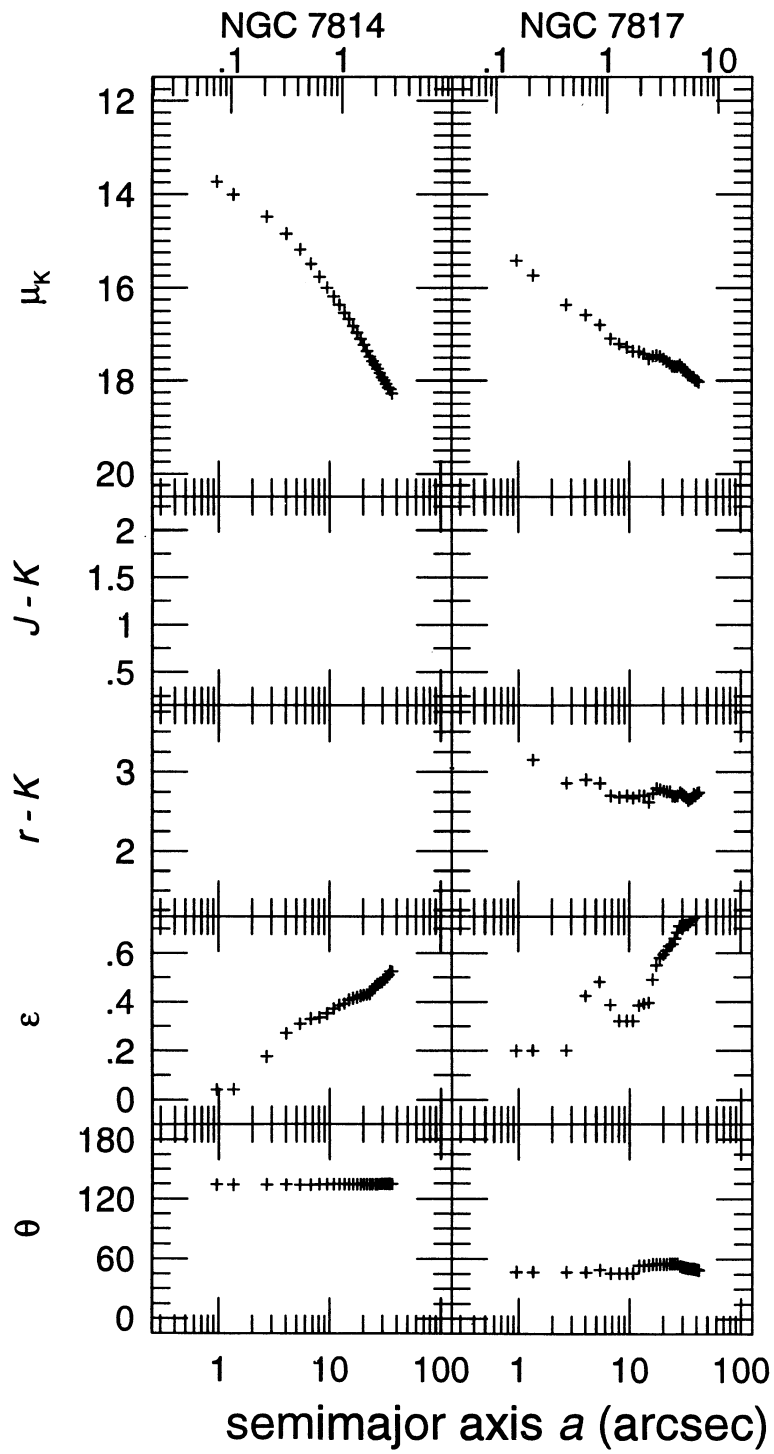

FIG. 5—*Continued*

TABLE 2

BULGE AND DISK COLORS AND COLOR GRADIENTS

				Bulge color		Disk color		Bulge color gradients				Disk color gradients			
NGC	a_b	a_d	r_d	$r-K$	$J-K$	$r-K$	$J-K$	$\delta(r-K)$	error	$\delta(J-K)$	error	$\delta(r-K)$	error	$\delta(J-K)$	error
128	5	20	15.0		0.90		0.90			−0.05	0.02			−0.16	0.40
474	10	10	10.5	2.25	0.80	2.05	0.85	−0.23	0.11	−0.18	0.05				
670	5	10	10.0	2.44	0.94	2.24	0.89	0.36	0.17	−0.25	0.06	−0.56	0.36	−0.05	0.17
697	5	20	18.5	2.58		2.33		0.68	0.24			−0.43	0.20		
753	5	8	11.0:	2.03		1.93		0.00	0.25			−0.90	0.46		
801	5	10	15.0	2.24	0.95	2.19	0.90			0.07	0.12	−0.14	0.16		
1023	10	15	26.0:		0.81		0.66			−0.16	0.05			−0.30	0.39
1035	5	15	20.5	2.28	1.01	2.03	0.86					0.07	0.40		
1087	3	10	13.0	1.65		1.35									
1325	7	15	30.0	2.58		2.48		−0.13	0.20						
1417	6	20	13.5:	1.98	0.80	1.68	0.70	−0.01	0.11	−0.15	0.05				
1620	5	20	28.5	2.07		1.92		0.17	0.23			−0.76	0.39		
2681		13	23.0:		1.12		1.20			−0.16	0.03			0.73	0.27
2715	7	10	34.5:	1.72		1.72									
2742	5	8	38.5:	1.97		1.67						−0.23	0.19		
2841	6	10	29.5:	2.59	0.96	2.69	0.96	−0.80	0.08	−0.26	0.06	0.17	0.03	0.00	0.04
2903	5	10	23.0	2.57		1.97						−0.23	0.14		
3198	5	10	26.5:	1.96		1.71									
3495	5	10	34.0:	1.86		1.86						−0.12	0.19		
4062	6	15	43.5:	2.07		2.12									
4448	15	15	15.0	1.75		1.75		−0.22	0.08			0.68	0.30		
4800	10	10	15.0	2.06		1.96		−0.41	0.10			−0.28	0.37		
5033	10	20	14.0	2.50	1.23	2.75	1.43	−0.29	0.07	0.09	0.06	0.38	0.14	0.27	0.17
7217	10	20	22.5	1.95	0.79	1.85	0.74	−0.10	0.03	−0.04	0.02	−0.67	0.24	−0.28	0.28
7331	8	30	32.0	2.13	0.78	2.38	0.98	−0.39	0.03	0.06	0.03	0.56	0.19	0.63	0.21
7332	8	25	15.0:		1.08		0.93			−0.30	0.04			0.21	0.15
7448	8	15	13.0	1.84	0.76	1.64	0.71	−0.12	0.12	0.08	0.06	0.41	0.48	0.02	0.16
7457	7	20	22.5:		0.83		0.98			−0.04	0.06				
7469	10	10	7.5:	2.02		1.62		−1.80	0.08			−1.47	0.44		
7537	4	10	12.5	2.03	0.84	1.98	0.94	0.44	0.30	0.05	0.15	−0.37	0.23	−0.08	0.26
7541	4	15	23.5:	2.59	1.16	2.44	1.01	−0.57	0.23	−0.81	0.09	−0.16	0.27	−0.07	0.32
7606	10	25	30.5	1.68		1.68		−0.10	0.08						
7631	4	10	14.0	1.88		1.93		−0.14	0.28			−0.67	0.32		
7664	5	10	7.5:	1.96	0.92	1.91	0.77	0.58	0.16	−0.32	0.06	−0.27	0.45	−0.24	0.50
7673		5	9.0:			2.45	0.72								
7798	5	10	10.5	1.99		1.79		0.15	0.20			0.05	0.46		
7817	8	20	36.0	2.35		2.25		−0.44	0.09			−0.28	0.06		

NOTES.—Bulge and disk colors in cols. (5)–(8) are corrected for Galactic extinction and internal absorption as described in the text. See § 3.4 for the definition of the color gradients.

disk colors were estimated from a radius a_d out to the last plotted point in the profile.[8] Note that these colors are azimuthally averaged, as measured by the major-axis profile, and are not aperture measurements on the images. The bulge and disk colors are summarized in Table 2, columns (5)–(8) of which list the mean bulge and disk colors, corrected for Galactic absorption and internal extinction as discussed below.

Column (4) of Table 2 lists a characteristic scale length r_d for the disks in our sample. This was measured by computing the e-folding length of the surface brightness profiles for $a \geq a_d$. About half the sample have outer profiles that are exponential, and for these the errors in r_d are $\pm 4''$. Many other galaxies, such as early-type systems or those for which the profiles could not be traced very far, show significant deviations from exponential profiles (cf. Kent 1985). The scale length for these galaxies, which are marked with a colon in column (4) of Table 2, have a larger error ($\pm 15''$). From a comparison of r_d to a_d and the maximum radius of the brightness profiles (Fig. 5), we note that we are measuring the colors in the disk over a range in radii that extends on average from 0.8 to $1.8 r_d$.

The first correction to the measured colors was for Galactic reddening, where we used an absorption-free polar cap model (Sandage 1973) where $A_V = 0.1(\mathrm{cosec}\, b^{\mathrm{II}} - 1)$ for $b^{\mathrm{II}} < 50°$ and $A_V = 0$ otherwise. Colors corrected for Galactic extinction will be denoted with subscript "0" (in Table 2, the subscripts are left off the column headings for clarity). We took A_V/A_B, $E(r-K)/A_V$, and $E(J-K)/A_V$ to be 0.78, 0.71 and 0.17, respectively (Cohen et al. 1981), and we took the effective wavelength of the r band to be essentially the same as that of Cousins R_C.

The second correction to the colors was to account for absorption internal to the galaxies themselves as a function of inclination angle, following the precepts in RSA. (Inclination corrected colors will be denoted with a subscript "0, i".) The RC3 values for axial ratio correlate strongly with the

[8] The reader may question at this point why we are not first decomposing the profiles into bulge and disk components, then measuring colors for the two components separately. Many of the profiles do not look like the sum of an exponential disk and a power-law or $r^{1/4}$-law bulge. Even for those that do, the decomposition is not always unique: compare, for example, the treatments in Kent (1985, 1986) and in Schombert & Bothun (1987). We therefore decided to pursue this simple approach here and leave the details of decomposition for subsequent papers. Our determination of the radii a_b and a_d were in part guided by preliminary decompositions of the major-axis profiles.

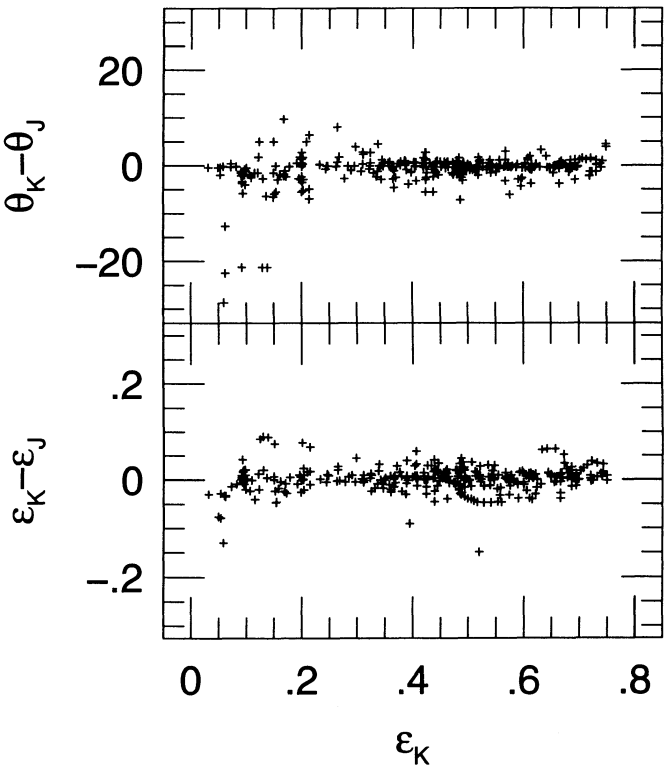

FIG. 6.—Differences between the ellipticity and position angle of the major-axis profiles measured at J and K are shown as functions of the ellipticity at K, ϵ_K. These are derived from the data presented in Fig. 5, and show the differences for all galaxies imaged in both J and K.

maximum ellipticity measured in our profiles, as shown in Figure 8. This demonstrates that even with small arrays we are able to measure the profiles to a large enough radius that the disk dominates the light. In this discussion, we subsequently adopt the RC3 values of axial ratio.

That the correction for inclination is significant is demonstrated in Figure 9, which illustrates the dependence of the bulge and disk colors (*top and middle panels, respectively*) on axial ratio. The colors in Figure 9 have been corrected for galactic absorption only. Bulge colors are shown as triangles, while disk colors are displayed as circles. In this and all subsequent figures which involve bulge colors, those galaxies which are judged to have an insignificant bulge component are not included. Colors measured under photometric conditions are shown as filled symbols, while those obtained under non-photometric conditions are shown as open symbols. There does not seem to be a significant difference in the distribution of colors of the filled and open points; if, for example there was a significant reduction in the K flux from clouds, then the derived $r-K$ color would be too blue. The lower panel of Figure 9 shows the correlation between inclination angle and $(V-K)_0$ color of Sc galaxy nuclei as given by Frogel (1985) in his Table 4. These colors were measured using apertures with a similar distribution in $\log(A/D_0)$ to that of the bulge-dominated regions in our present sample.

The straight lines in Figure 9 show the expected dependence of color with inclination angle for early and late type spirals as summarized in the RSA. Extinction values and color excess ratios as given by Cohen et al. (1981) were employed. The reddening lines were shifted in color to overlap the average observed bulge and disk colors of those galaxies with $(r-K)_0 \leq 2.6$. In Figure 9, galaxies with disk or bulge colors $(r-K)_0 \leq 2.6$ show the expected dependence of color with inclination angle, albeit with considerable scatter. Both Aaronson (1979) and Griersmith et al. (1982) found only a weak dependence of color on flattening, but their samples of galaxies contained very few highly flattened or late-type spirals. This is also true of the Frogel (1985) sample of Sc galaxies.

About one-quarter of the galaxies plotted in Figure 9 have $(r-K)$ colors significantly redder than expected from their inclination angles. Aaronson and Griersmith et al. identified a similar population of red galaxies in their samples; we will discuss these galaxies later.

3.2. *Bulge and Disk Colors Compared*

In Figure 10 we plot the correlation between bulge and disk colors in $(r-K)_{0,i}$ and $(J-K)_{0,i}$. The symbols in Figure 10 are as in Figure 9, and the solid lines denote identical colors. Figure 10 suggests that the colors of the bulges and disks may be correlated; the correlation is stronger in $J-K$ than in $r-K$. In $J-K$ the bulges and disks have nearly identical colors, while in $r-K$ the bulges tend to be ~ 0.1 mag redder than the disks. The scatter in these correlations is comparable to or only slighter greater than expected from the measuring uncertainties alone which are 0.06 mag (§ 2.5). These results are independent of the inclination corrections that have been applied since the same correction was applied to both the bulge and disk colors.

In Figure 11 we show the correlation between $(r-K)_{0,i}$ and $(J-K)_{0,i}$, for bulges and disks considered together. The bulge and disk points for individual galaxies are connected by lines. The arrow denotes the effects of 0.5 mag of visual extinction, while the points connected by dashed lines show model colors for single-burst populations of age 12×10^9 yr and [Fe/H] (from blue to red) of -1.0, -0.5, and 0.0 dex (Worthey 1992). The range in the bulge and disk colors lie along either the reddening or metallicity line, which are nearly parallel. We will discuss the interpretation of these colors below (§ 4.1).

3.3. *Bulge and Disk Colors as Functions of Galaxy Type*

In Figure 12 we plot the distributions of inclination-corrected bulge and disk colors as a function of Hubble type T. The symbols in Figure 12 are the same as in Figures 9–11. With the exception of a 0.1 mag difference in $(r-K)_{0,i}$ (also seen in Fig. 9), there are no obvious differences between the colors of bulges and disks of a given type. The $(r-K)_{0,i}$ colors for both the bulges and the disks of late-type galaxies are a few tenths of a magnitude bluer than those of earlier systems, while the $(J-K)_{0,i}$ colors are nearly independent of T.

There is a reasonably well defined lower limit to $(r-K)_{0,i}$ for galaxies with $T \geq 1$ that may get slightly bluer with advancing type. There also appears to be a fairly constant lower limit for $(J-K)_{0,i}$. The upper limit to $(r-K)_{0,i}$, on the other hand, gets significantly redder with advancing type; the upper limit to the $(J-K)_{0,i}$ colors may get redder as well. These red galaxies are the same ones that stand apart from the general trend with inclination angle displayed in Figure 9. The net result of this is that the dispersion in colors increases markedly with advancing T class.

We now compare the mean colors of our galaxies against those of early-type systems measured by Persson, Frogel, & Aaronson (1979) and to those of Sc nuclei in Frogel (1985). Persson et al. (1979) obtained *UBVRJHK* photometry of a large number of E and S0 galaxies; these systems show a very

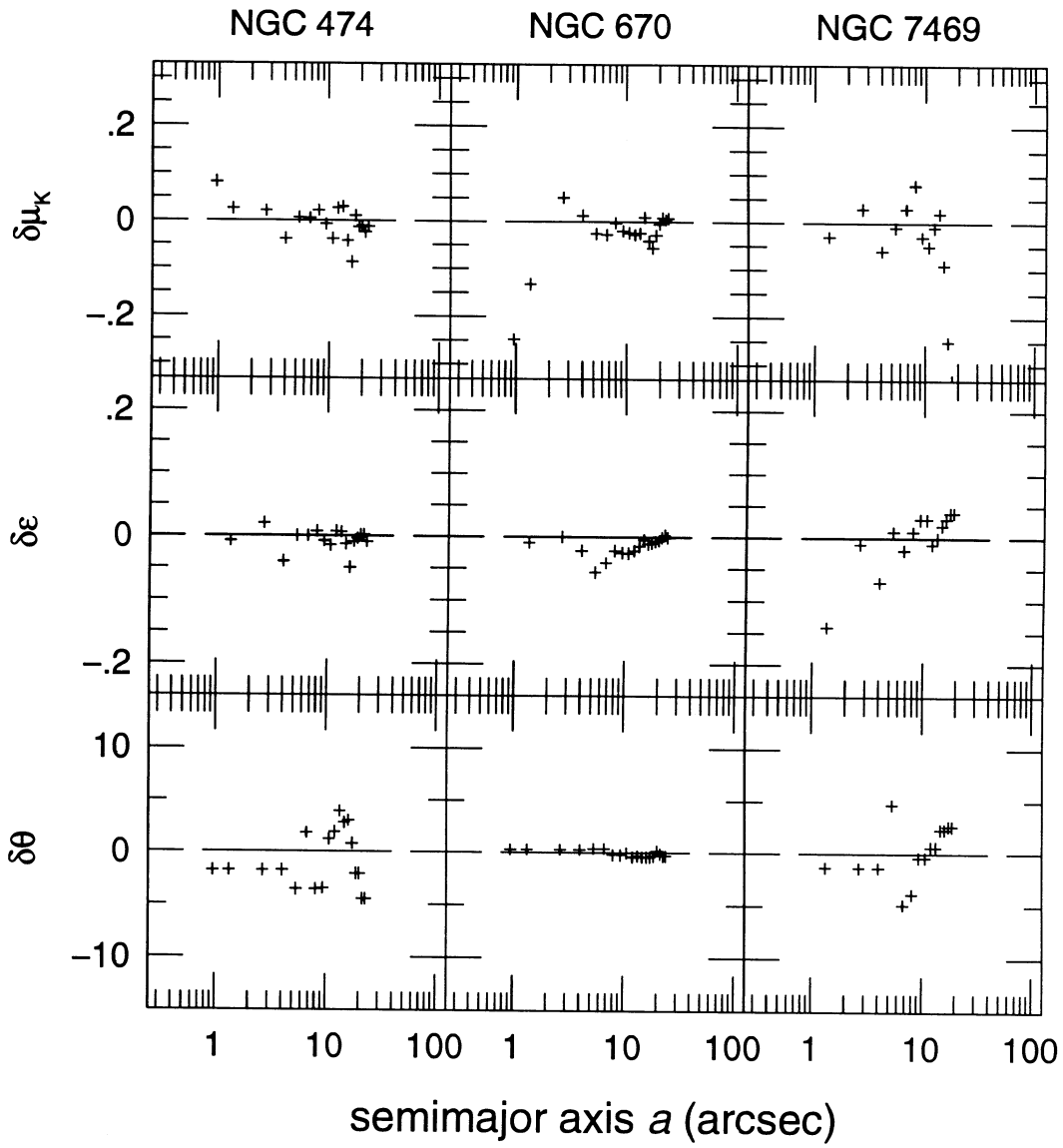

FIG. 7.—This figure illustrates the results of independent surface brightness measurements of three of the galaxies in the sample. The two sets of measurements being compared for each of the galaxies were obtained on different nights or on different telescopes. From top to bottom are plotted the differences in K major-axis surface brightness, ellipticity, and position angle. The differences are in the sense of the illustrated data (Fig. 5) *minus* data from the repeat observations.

narrow range of $r-K$ colors, with a mean $(r-K)_0 = 2.48$ and a dispersion of only 0.16 mag (we take $R-K$ to be identical to $r-K$). This is similar to the bulge colors of the S0 galaxies in our sample, but markedly redder than the colors of the later type systems.

In Figure 13 we display the $(J-K)_{0,i}$ and $(V-K)_{0,i}$ colors of Sc nuclei from Frogel (1985), where we have corrected Frogel's colors for inclination in the same fashion as for our sample. We find that in the mean the $(J-K)_{0,i}$ colors of Frogel's galaxies are very similar to those of the late-type systems presented here, and that the Sc nuclei extend the relation between color and type to redder types.

3.4. *Color Gradients*

We measured color gradients in the bulges and disks by computing the slopes $\delta(J-K) \equiv d(J-K)/d \log a$ and $\delta(r-K) \equiv d(r-K)/d \log a$ via least squares over the radius ranges $a \leq a_b$ and $a \geq a_d$, respectively. Note that as with the determination of the mean colors, these gradients are measures of the azimuthally averaged major-axis profile. The fit was performed using $1/\sigma^2$ weighting, where σ is the error of the color. The color gradients and errors are given in columns (9)–(16) of Table 2. Gradients with errors larger than 0.5 have been deleted. In general, the errors of the color gradients of the bulges are smaller than those for the disks because of higher signal-to-noise in the bright inner parts of the profiles.

The color gradients are displayed for bulges and disks separately as a function of Hubble type in Figure 14. Unlike in Figures 9–11, there is no distinction in the figure between galaxies observed under photometric conditions and those that were not, since the value of the gradient does not depend on the measured flux in the galaxy.

Most bulges and disks with $T \leq 4$ exhibit negative gradients, i.e., bluer colors outward. In late-type systems, there is

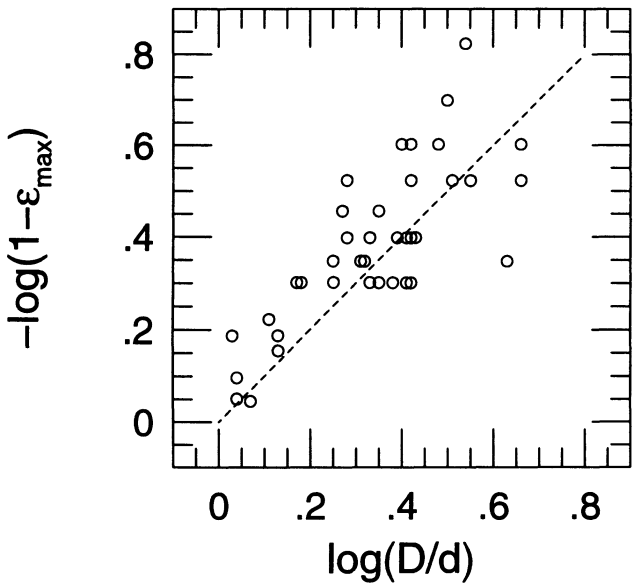

FIG. 8.—Comparison of axial ratio at the outermost measured isophote in our observations (*vertical axis*) against the axial ratio tabulated in the RC3. The dashed line shows equality.

an increasing fraction of galaxies that have positive gradients (redder outward). The average bulge gradient for all types of galaxies is $\delta(J-K) = -0.07$ and $\delta(r-K) = -0.12$. Gradients in the disks show a large scatter, though more disks have negative gradients than positive gradients. There is no correlation between the sizes of the color gradients and the colors of the bulges or disks.

In Figure 15 we show the correlation between the color gradients in $J-K$ and those in $r-K$ for bulges and disks. The arrows show the reddening vector for 0.5 mag of visual extinction, while the points connected by a solid line show the color changes in Worthey's (1992) models of age 12×10^9 yr as the metallicity changes in steps of 0.5 dex from (*left to right*) [Fe/H] $= -1.0$ to $+0.5$. As we found with the colors themselves (Fig. 11), the color gradients that would be produced by a change in metallicity are parallel to those from a change in the internal extinction within the galaxy.

4. DISCUSSION

4.1. *Comparison with Evolutionary Models and Optical Photometry*

Worthey (1992) has calculated an extensive grid of integrated colors of single-age, single-metallicity populations which we now compare to the bulge and disk colors and color gradients discussed above. We find an average color difference between disks and bulges of 0.1 mag in $r-K$ and ~ 0 in $J-K$; the sense of the difference is that the bulges are redder than disks. For Worthey's solar abundance models these color differences correspond roughly to a difference in abundance of 0.1 to 0.2 in [Fe/H] *or* approximately 2–4 billion years in the mean age of the stellar components, the disks being younger or more metal-poor.

We remind the reader that we are only sampling the inner disks of the galaxies in our sample (see Fig. 5). If galaxies have continually declining disk metallicities with radius as in the Milky Way, then colors measured farther out in the disks might show larger differences from the bulge colors. Nevertheless, in contrast to marked differences that are seen in the optical, our new data show that at infrared wavelengths the bulk of the stellar content of the bulges and inner disks of spiral galaxies are similar. This extends an earlier result (Frogel 1985) that the near infrared light of the nuclei of Sc galaxies is dominated by an old stellar population not unlike that found in E and S0 galaxies.

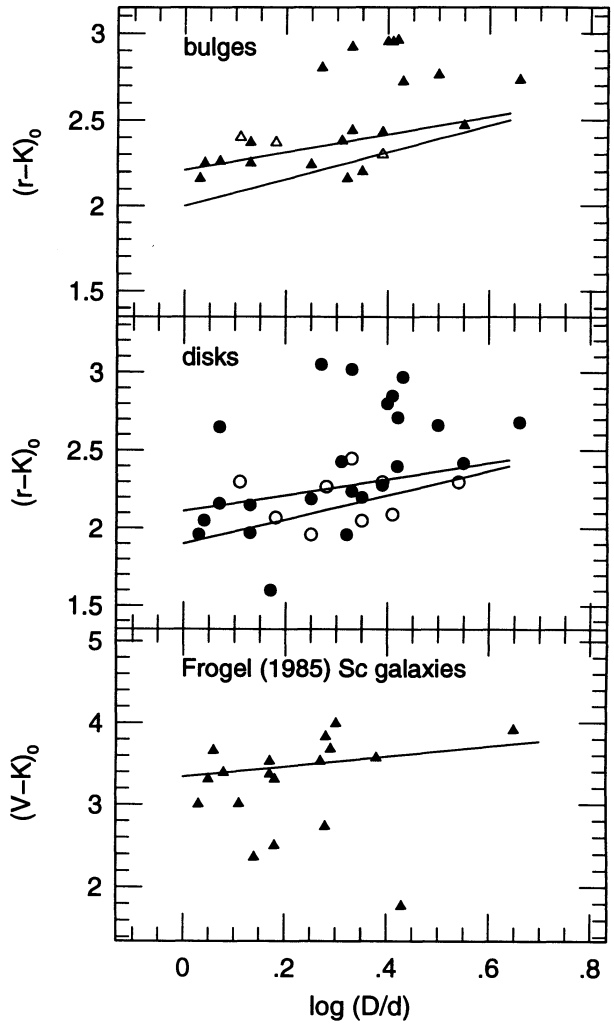

FIG. 9.—Dependence of bulge and disk colors on inclination angle. the top and central panels, respectively, show the bulge and disk $(r-K)_0$ colors corrected for Galactic absorption only. Filled points indicate photometricaly calibrated colors, while the open symbols denote colors measured under slightly nonphotometric conditions. The straight lines are the predicted relations from the RSA for early and late type disk systems inclined by varying degrees to the line of sight. The bottom panel shows a similar plot for $(V-K)_0$ colors of the Sc nuclei in Frogel (1985). No corrections for internal extinction have been applied to the data in these panels.

We found above that for $T \leq 2$, the bulge colors are similar to but slightly bluer than ellipticals and lenticulars. This would easily be explained if the bulges have a somewhat lower metallicity and/or mean age than do the ellipticals, perhaps as a consequence of a lower luminosity. Balcells & Peletier (1993) have investigated bulge colors and color gradients in a sample of 45 early-type spirals observed in *UBRI*. They select a subset of spirals that are relatively unaffected by dust, and demonstrate that the colors of the bulges are generally bluer than those of ellipticals, consistent with our findings in this paper.

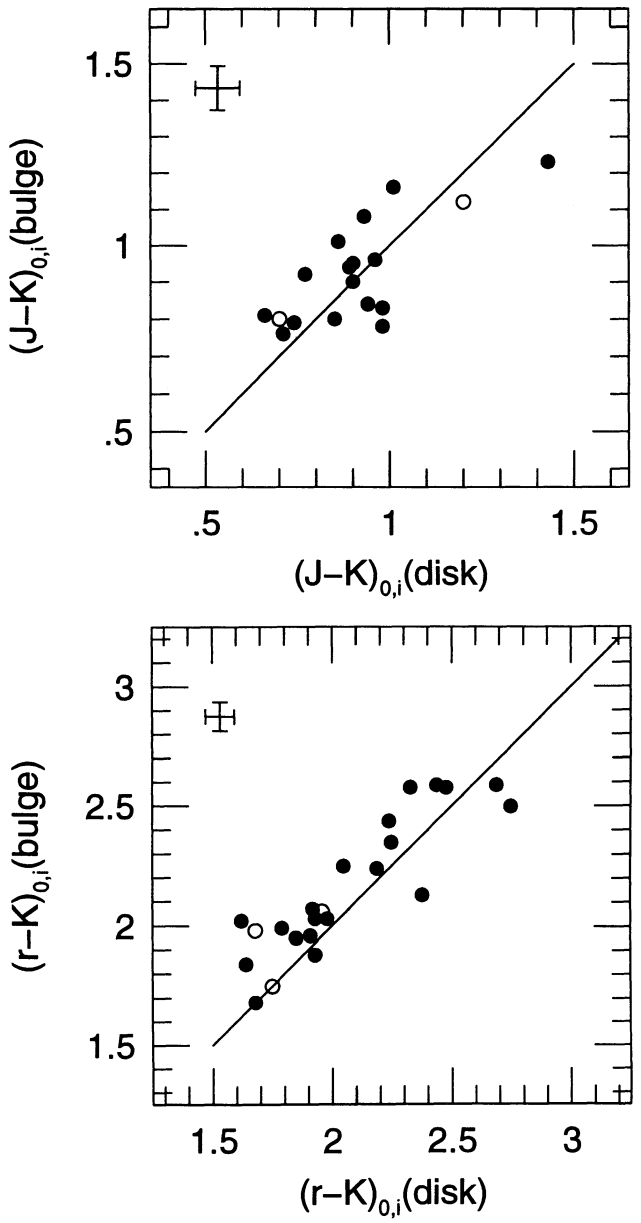

FIG. 10.—Two panels of this figure illustrate, for the $r-K$ and $J-K$ colors separately, the correlation between bulge and disk colors. Lines of equality are indicated. The error bars of ± 0.06 mag in each color are based on the comparison of our data with published aperture photometry as discussed in § 2.5. Filled and open symbols are as in Fig. 9.

With only *rJK* colors at our disposal, we were not able to distinguish color changes caused by extinction from those produced by metallicity gradients. The full span of colors and color gradients exhibited by the galaxies can be accounted for by either a variation in internal extinction by $A_V \sim 1$ about the mean values found optically as a function of inclination angle, or by variations in metallicity of order 1 dex from galaxy to galaxy. For example, we found that the mean color change within bulges is on the order of -0.1 in $r-K$ which corresponds in Worthey's models to decline in metallicity of approximately 0.2 dex. This is similar to the gradient of metallicity in the bulge of the Galaxy (Terndrup 1988; Frogel et al. 1990; Terndrup, Frogel, & Whitford 1990).

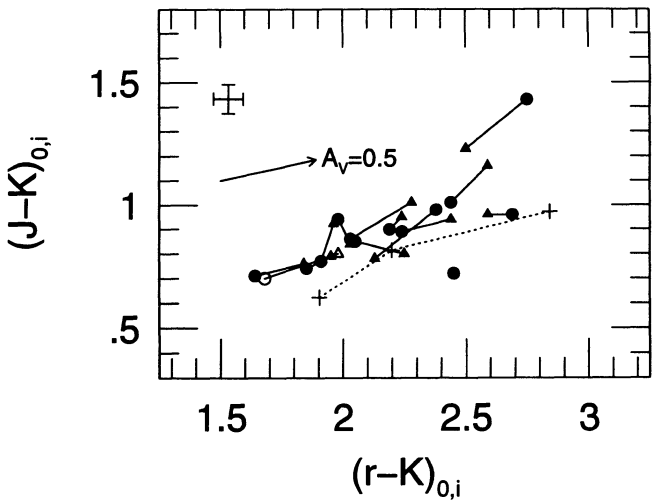

FIG. 11.—This figure illustrates the correlation between the $J-K$ and $r-K$ colors for the bulges and disks. The short solid lines connect points representing the bulge color (*triangles*) to the disk color (*circles*) for individual galaxies. Filled and open symbols are in Figs. 9 and 10. The arrow displays the effect of 0.5 mag of internal visual extinction. The plusses connected by a dashed line show predicted colors from Worthey (1992) for single-burst populations of age 12×10^9 yr for mean metallicity (from blue to red colors) of [Fe/H] = -1.0, -0.5, and 0.0, respectively.

So far we have applied Worthey's models differentially, If we use the mean bulge and disk colors in Figure 11, we conclude that most bulges have abundances on the order of -0.5 dex, with few achieving solar abundances. At first sight, this may seem to contradict the results from several investigations of the Milky Way's bulge (e.g., Frogel 1988; Rich 1988; McWilliam & Rich 1994) which all conclude that the mean metallicity of the bulge is approximately solar. On the other hand, this difference may simply mean that Worthey's simple models predict

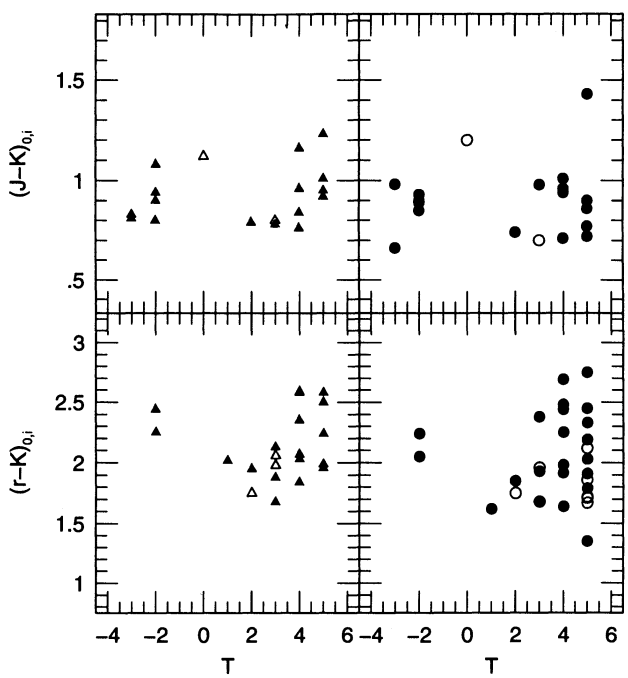

FIG. 12.—Bulge (*left panels*) and disk (*right panels*) colors as a function of galaxy type, after correction for internal extinction as described in the text. Filled and open circles are as in Fig. 9.

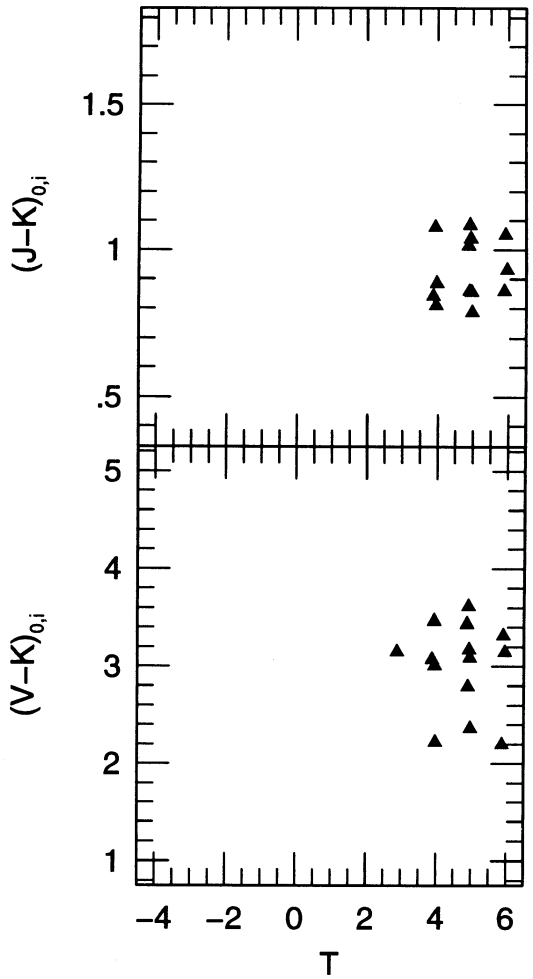

FIG. 13.—Central colors for Sc nuclei measured by Frogel (1985), plotted as a function of galaxy type.

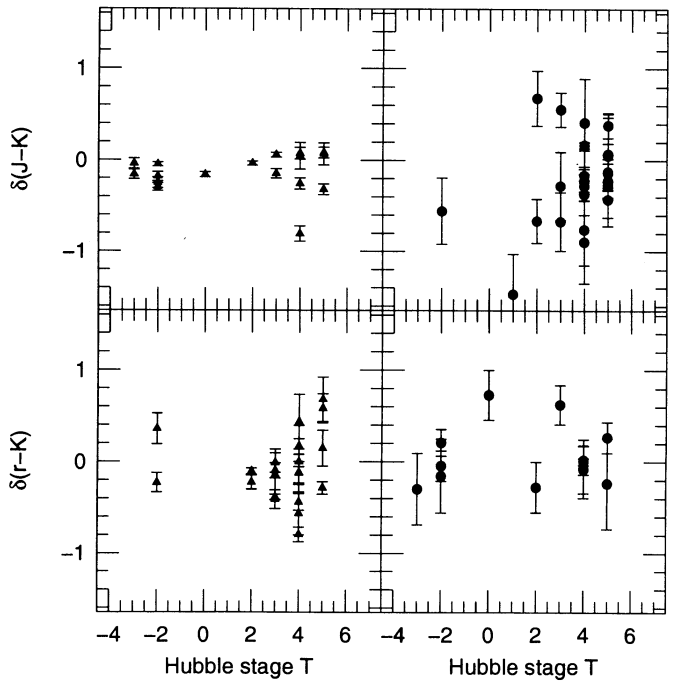

FIG. 14.—Color gradients for bulges (*triangles*) and disks (*filled circles*) plotted as a function of galaxy type. See § 3.4 for the definition of the gradients. A positive value indicates that the color becomes bluer with increasing radius in the galaxy.

colors that are somewhat too red at a given metallicity, so using his models would underestimate the mean abundance.

The behavior of the bulge color gradients that we find is similar to that shown optically by Balcells & Pelletier (1993). They find that the magnitude of the color gradient is larger in high-luminosity bulges, and that the gradients in faint bulges (corresponding to $T > 4$) scatters widely with an average gradient having a negative value. They also find that few bulges reach solar metallicities, which is also consistent with our conclusions drawn above.

4.2. *The Red Galaxies*

In Figure 9 we noted that several galaxies have bulge and disk colors that are 0.5 mag redder in $(r - K)_{0,i}$ than expected for their inclination angle. With the exception of NGC 7331 at $T = 3$, all of the other red galaxies have $T = 4$ or 5. They are therefore the reddest galaxies of their type and occupy the upper parts of the color distribution in Figure 10. As may be seen from Figure 9, many of these systems have high inclination angles and are therefore nearly edge-on (cf. Fig. 1). This could mean that internal reddening plays a significant role in producing these extra-red galaxies. Both Aaronson (1977, 1979) and Griesmith et al. (1982) identified similar red subsets of their samples but suggested that a combination of continuous emission from obscured regions of young stars and associated emission lines would account for the red colors.

We have attempted to ascertain whether the red galaxies in our sample have active nuclear regions due to star formation or nonthermal activity by examining fluxes from the *IRAS* Catalogued Galaxies and Quasars (Fullmer & Lonsdale 1989). Three quantities were investigated: the ratio of 100 μm to 60 μm flux, the ratio of far-IR to blue luminosity, and the absolute far-IR luminosity. We took fully corrected blue magnitudes from the RSA or RC3. Figure 16 shows these three quantities plotted against the reddening and inclination corrected $r - K$ color. There is no hint that any of these quantities are different for redder disks and bulges than for blue ones. Furthermore there *are* several well-known active galaxies in our sample. NGC 2903 is a "hotspot" galaxy with a nuclear starburst. Its appearance leads us to call it nearly edge-on, yet the $r - K$ color of its disk is more than 0.5 mag *bluer* than our red galaxies. NGC 7469 is a Seyfert with circumnuclear star formation. Its disk and bulge colors are typical for its nearly face-on orientation. NGC 7541 is the only galaxy in our red sample known to be active—it has a nuclear starburst. Thus while we cannot rule out that there is hidden, i.e., heavily obscured nuclear activity in our red galaxies, we regard this explanation as unlikely.

We suspect that the main source of the red colors seen in a subset of our galaxies and by Aaronson (1977, 1979) and Griersmith et al. (1982) is internal extinction over and above that predicted by the formula we have used for extinction corrections based on inclination angle alone. There are two ways this situation can arise, both of which are expected to be relevant for late-type galaxies: (1) the internal extinction is variable over a resolution element of the observations, and/or (2) the dust is mixed in with the stars rather than acting as a screen. In

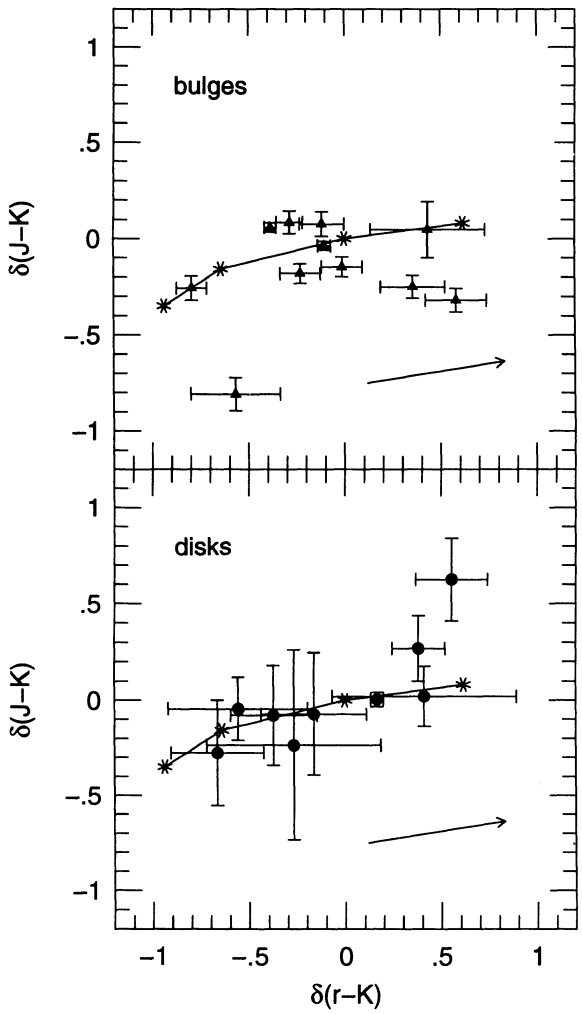

FIG. 15.—Color gradients in $J-K$ against those in $r-K$ for bulges (*top panel*) and disks (*lower panel*). The arrow designates the effects of 0.5 mag of visual extinction. The asterisks show the effect of a change of metallicity of (from blue to red) -1.0, -0.5, 0.0, and $+0.5$ dex in Worthey's (1992) models.

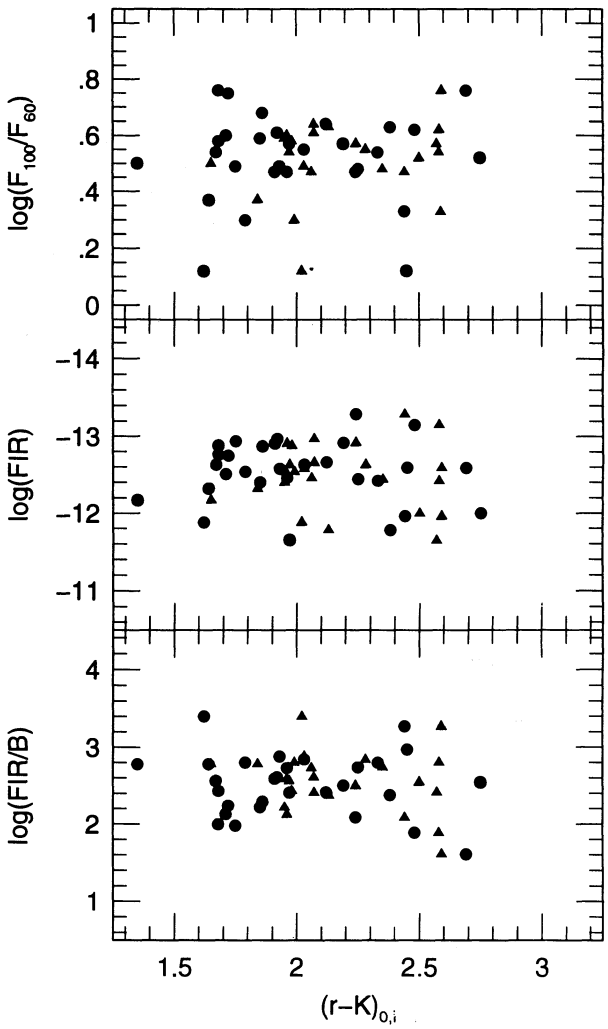

FIG. 16.—Three potential measures of nuclear activity are shown plotted against $(r-K)_{0,i}$. The 100 to 60 μm flux ratio and the far-IR luminosity are from the *IRAS* Catalogued Galaxies and Quasars (Fullmer & Lonsdale 1989). $H_0 = 75$ km s^{-1} Mpc^{-1} was used. Blue luminosities are from the RSA or from the RC3. Bulge colors are plotted as triangles, while the disk colors are shown as filled circles.

both cases the infrared radiation will contain a larger component from light that is heavily obscured than will optical light. Frogel (1985) discusses this in more detail. He also noted that for Sc nuclei in common with Turnrose (1976), the latter's predictions for extinction based on stellar synthesis models agree well with his observations. These extinction values were several times greater than those estimated from the inclination effect alone.

5. CONCLUSIONS

We present imaging surface photometry in J and K for a sample of 43 spiral and S0 galaxies drawn from the RSA with optical CCD photometry from Kent (1984, 1986, 1987). This study was carried out with a 58 × 62 InSb array and establishes the feasibility of the extensive survey of spirals we are now undertaking with 256 × 256 devices. We demonstrate that we can measure surface brightness down to fainter than $K = 19$ mag arcsec^{-2} to a precision of 20%. This is typically 250 times fainter than the night sky at K. Magnitudes measured through synthesized apertures on our images agree with the best existing photoelectric aperture photometry to within 0.2% in J, 0.6% in H and 1.6% in K.

We report azimuthally averaged K-band luminosity, $J-K$ and $r-K$ color profiles, and the run of ellipticity and position angle with radius. The luminosity profiles exhibit structure corresponding to changes in ellipticity which allow the disk and bulge components to be separated. The ellipticity profiles increase monotonically with radius as the disk component dominates in surface brightness. The position angles show little variation.

In contrast to optical wavelengths where blue light from young stars has a major effect on disk colors, we find that the near-IR colors of the bulge and disk components are very similar. This indicates that the red stellar content of both components is similar in age and metallicity. In the mean the disks are 0.1 mag bluer in $r-K$ than bulges; a rudimentary comparison with Worthey's (1992) models suggests that this would arise if the disks are 2–4 billion years younger or Δ[Fe/H] $= -0.1$ to -0.2 more metal poor than the bulges. The color gradients in the bulge imply metallicity gradients of a few tenths dex as found in the bulge of the Milky Way.

The colors of the bulges for late-type galaxies are similar but

slightly bluer than those in early-type systems, as would be expected for lower bulge luminosities if luminosity and metallicity are correlated. In the later Hubble types ($T > 2$) there is a broader spread in bulge and disk colors than in earlier types, and there are a substantial number of galaxies, amounting to 25% of the sample, which are redder by as much as $r - K = 0.5$ mag than more typical galaxies. Examination of the correlation between color and inclination angle suggests that the red colors of these galaxies can in part be accounted for by larger internal extinction, but not by nuclear or starburst activity. On the other hand, the red colors can also be explained by higher metallicities, up to 0.5 dex above the average metallicity for the galaxies with normal colors.

This project was partially supported by NSF grant AST 92-17716 to The Ohio State University. J. A. F.'s research is supported in part by NSF grant AST92-18281. D. M. T. received some support from NSF grant AST91-57038. J. A. F. thanks Leonard Searle for the hospitality he received at the Las Campanas Observatory. R. L. D. acknowledges the support of the University of Oxford Astronomy Astor travel fund for supporting his visit to The Ohio State University and the support of the SERC visitors grant to Oxford Astrophysics for supporting visits by J. A. F. and D. M. T. We thank Gary DaCosta, Steve Kent, Richard Pogge, and Alice Quillen for helpful comments. The referee, Greg Bothun, suggested several critical modifications and clarifications which have been incorporated into the discussion. This research has made use of the NASA/IPAC Extragalactic Database (NED), which is operated by the Jet Propulsion Laboratory, Caltech, under contract with the National Aeronautics and Space Administration.

REFERENCES

Aaronson, M. 1977, Ph.D. thesis, Harvard Univ.
———. 1979, ApJ, 221, L103
Aaronson, M., et al. 1982, ApJS, 50, 241
Aaronson, M., Mould, J., Huchra, J., Sullivan, W. T., Schommer, R. A., & Bothun, G. D. 1980, ApJ, 239, 12
Balcells, M., & Peletier, R. F. 1993, preprint
Bothun, G. D., Aaronson, M., Schommer, B., Mould, J., Huchra, J., & Sullivan, W. T. 1985, ApJS, 57, 423
Bothun, G. D., & Gregg, M. D. 1990, ApJ, 350, 73
Cohen, J. G., Frogel, J. A., Persson, S. E., & Elias, J. H. 1981, ApJ, 249, 481
de Vaucouleurs, G., de Vaucouleurs, A., Corwin, H. G., Buta, R. J., Paturel, G., & Fouqué, P 1991, Third Reference Catalog of Bright Galaxies (New York: Springer) (RC3)
Elias, J. H., Frogel, J. A., Matthews, K., & Neugebauer, G. 1982, AJ, 87, 1029
Fowler, A. M., Gillett, F. C., Gregory, B., Joyce, R. R., Probst, R. G., & Smith, R. 1987, in Proc. Workshop on Ground-Based Astronomical Observations with Infrared Array Detectors, ed. C. G. Wynn-Williams & E. E. Becklin (Hilo: Univ. Hawaii), 197
Franx, M., Illingworth, G., & Heckman, T. 1989, AJ, 98, 538
Frogel, J. A. 1985, ApJ, 298, 528
———. 1988, ARA&A, 26, 51
Frogel, J. A., Persson, S. E., Aaronson, M., & Matthews, K. 1978, ApJ, 220, 75
Frogel, J. A., Terndrup, D. M., Blanco, V. M., & Whitford, A. E. 1990, ApJ, 353, 494
Frogel, J. A., & Whitford, A. E. 1987, apJ, 320, 199
Fullmer, L., & Lonsdale, C. 1989, Catalogued Galaxies and Quasars Observed in the *IRAS* Survey, Version 2 (Pasadena: JPL)
Gregg, M. D. 1989, ApJ, 337, 45
Griersmith, D., Hyland, A. R., & Jones, T. J. 1982, AJ, 87, 1106
Hackwell, J. A., & Schweizer, F. 1983, ApJ, 265, 643
Jedrzejewski, R. I. 1987, MNRAS, 226, 747
Kent, S. M. 1984, ApJS, 56, 105
———. 1985, ApJS, 59, 115
———. 1986, AJ, 91, 1301
———. 1987, AJ, 93, 816
Lauer, T. R. 1985, ApJS, 57, 473
McWilliam, A., & Rich, R. M. 1994, ApJS, 91, 749
Peletier, R. F., Davies, R. L., Illingworth, G. D., Davies, L. E., & Cawson, M. 1990, AJ, 100, 1091
Persson, S. E., Frogel, J. A., & Aaronson, M. 1979, ApJS, 39, 61
Rich, R. M. 1988, AJ, 95, 828
Rix, H.-W. 1993, PASP, 105, 999
Rix, H.-W., & Rieke, M. J. 1993, ApJ, 418, 123
Sandage, A. 1961, The Hubble Atlas of Galaxies (Washington: Carnegie Institution)
———. 1973, ApJ, 183, 711
Sandage, A., & Tammann, G. A. 1981, A Revised Shapley-Ames Catalog of Bright Galaxies (Washington: Carnegie Institution) (RSA)
Schombert, J. M., & Bothun, G. D. 1987, AJ, 93, 60
Scoville, N. Z., Matthews, K., Carico, D. P., & Sanders, D. B. 1988, ApJ, 327, L61
Stover, R. J. 1988, in Instrumentation for Ground-Based Optical Astronomy, ed. L. B. Robinson (New York: Springer), 433
Terndrup, D. M. 1988, AJ, 96, 884
Terndrup, D. M., Frogel, J. A., & Whitford, A. E. 1990, ApJ, 357, 453
Turnrose, B. E. 1976, ApJ, 210, 33
Worthey, G. 1992, Ph.D. thesis, Univ. California at Santa Cruz